BIOCHEMISTRY
including biophysical chemistry & molecular biology

Article

pubs.acs.org/biochemistry

Evaluation of Tyro3 Expression, Gas6-Mediated Akt Phosphorylation, and the Impact of Anti-Tyro3 Antibodies in Melanoma Cell Lines

Stephen J. Demarest,* Jennifer Gardner, Michelle C. Vendel,† Eric Ailor,‡ Suzanne Szak, Flora Huang, Adam Doern, Xiangyang Tan, Weixing Yang, Dorre A. Grueneberg, Edward J. Richards, Wilson O. Endege, Ed Harlow, and Louise A. Koopman*

Biogen Idec, 14 Cambridge Center, Cambridge, Massachusetts 02142, United States

Supporting Information

ABSTRACT: Tyro3, a member of the Tyro3/Axl/Mer (TAM) family of receptor tyrosine kinases, has emerged as a potential oncogene in melanoma. Here, we confirm that Tyro3 is specifically overexpressed in primary melanoma samples and show that Tyro3 is expressed at varying levels in numerous melanoma cell lines. Short hairpin RNA-mediated knockdown of Tyro3 led to significant cell death via apoptotic mechanisms in nearly all melanoma cell lines tested, regardless of the BRAF or NRAS mutation status or co-expression of Axl and/or Mer. We generated soluble and monomeric versions of the human Tyro3 extracellular domain and human Gas6 for affinity measurements and correlated these values with the level of Gas6 required to induce Tyro3 signaling in cellular assays. Calcium was critical for the correct folding of Gas6 and its binding to Tyro3. In melanoma cell lines, Gas6 induced Tyro3 phosphorylation and downstream Akt phosphorylation without apparent effects on Erk. We generated monoclonal antibodies (mAbs) against Tyro3 to examine their effect on survival signaling in melanoma cell lines. The mAbs generated against Tyro3 included nonligand blockers, partial blockers, and competitive ligand blockers. A number of weak and partial ligand blockers (all recognizing the Tyro3 Ig domains) were the most effective at blocking ligand-mediated downstream signaling of Tyro3. Overall, these data indicate that Tyro3 may confer increased survival signals in melanoma cells and can be stymied using inhibitory mAbs. These mAbs may be useful for further investigations of the role of Tyro3 in melanoma.

Tyro3 (also known as Sky, DTK, Rse, and Tif), Axl, and Mer play key roles in immunity and inflammation.[1] The receptors are collectively known as the TAM, TAMR, or Tyro3 family of receptor tyrosine kinases (RTKs) and are structurally homologous to one another, having sequences that are roughly 30% identical and 50% homologous. The receptors all contain an N-terminal extracellular domain consisting of two Ig fold domains and two type III fibronectin domains, followed by a single transmembrane helix and a cytoplasmic tyrosine kinase domain. With varying specificity and binding strengths, the receptors can be activated by the homologous ligands Gas6 or protein S (PS).[2,3] Ligand binding has been shown to lead to downstream activation of the phosphoinositide 3-kinase (PI3K)/Akt survival pathway and phospholipase C.[4] Each receptor also maintains unique associations with other signaling pathways that differentiate their activities within various tissues and cell types.[4−6]

The TAM receptors play overlapping as well as unique roles in regulating immunity and inflammation. Many of the roles of the TAMRs were inferred from the study of single, double, and triple TAMR knockout mice[7,8] and pertain to homeostatic maintenance in adult nervous, reproductive, and vascular tissues by phagocytosis of apoptotic cells. The TAMRs have also been shown to provide intrinsic regulatory feedback inhibition of innate immune responses (dendritic cells and macrophages). The triple knockouts are viable but demonstrate multiple debilitating and degenerative traits, most importantly, impaired hemostasis, immunoregulation, spermatogenesis, and blindness.[1] The highly negatively charged γ-glutamic acid terminal region of TAMR ligands PS and Gas6 is thought to bind phosphatidylserine on the surface of apoptotic cells, while the LG terminal domains bind the TAMRs. The bridge thus formed between apoptotic cells and cell types expressing TAMRs (e.g, retinal pigment epithelial (RPE) cells, Sertoli cells, and macrophages) facilitates phagocytosis and clearance. Of the three receptors, Mer has the most apparent role in the phagocytosis of apoptotic cells, with a lack of natural photoreceptor clearance, as well as less potent macrophage-mediated clearance in primary and secondary lymphoid organs, observed in MER knockout mice.[9] Blindness caused by an impaired RPE phagocytosis pathway is consistent with the blindness observed in MER knockout mice, as well as in individuals with retinal dystrophy in whom MER kinase domain mutations are found.[10] Axl plays a specific role in both the development of natural killer cells and the regulation of antigen-presenting cells via Toll-like receptor silencing.[1] The autoimmune phenotype resulting from hyperactivation of antigen-presenting cells due to release of the inhibitory

Received: November 27, 2012
Revised: April 8, 2013
Published: April 9, 2013

feedback regulation is mostly attributable to Axl, as evidenced when Axl is knocked down in dendritic cells.[11] In contrast, dendritic cells do not express Tyro3 (G. Lemke, personal communication). Consistent with its restricted expression mainly in brain and spinal cord, Tyro3 is thought to play a neuroprotective role by promoting neuronal survival and a reproductive function by stimulating migration of GnRH neurons to the forebrain.[6,12,13] In addition, Tyro3 has been shown to mediate osteoclastic bone resorption in mice.[14]

Axl and Mer have been implicated in tumor survival, invasiveness, growth, and even angiogenesis (Axl) for more than a decade.[4] Axl, in particular, has been shown to allow resistance to both HER-2 and EGFR inhibitors[15−17] in non-small cell lung, breast, and gastric tumors as well as resistance to chemotherapy and imatinib in acute myeloid leukemia.[18] Progress has been made in assessing the value of targeting Axl with both monoclonal antibody (mAb) and small-molecule kinase inhibitors for controlling tumor formation, growth, and invasiveness. Inhibitory mAbs against Axl were shown to increase the sensitivity of tumors to chemotherapeutics and, in combination with a small-molecule EGFR inhibitor or an anti-VEGF antibody inhibitor, to decrease the extent of breast and lung cancer xenograft growth.[19,20] A small-molecule Axl inhibitor, R428, demonstrated the ability to inhibit Axl-mediated Akt signaling, inflammatory cytokine production, and tumor metastases and increased the overall level of survival of breast tumor-bearing mice.[21] Additional small-molecule receptor tyrosine kinase (RTK) inhibitors in the clinic for the treatment of various cancers (including foretinib, carbozantinib, MP470, and others) have been found to cross-react with Axl, and it is believed that this additional activity could improve the therapeutic capacity of these entities.[22,23]

Early reports[24,25] that associated Tyro3 with tumorigenesis have only recently been further substantiated. In a cellular screen in which all RTKs were systematically knocked down, Tyro3 emerged (among several others) as being essential for cellular survival,[26] in keeping with the PI3K/Akt pathway activation reported after ligand stimulation.[27] Tyro3 was also identified among activated kinases in a phosphoproteomic screen in lung cancer.[28] It was proposed as a melanoma-specific oncogene in a gain-of-function genomic screen that sought to identify upstream regulators of microphthalmia-associated transcription factor (MITF-M), a gene linked to poorer patient outcome in melanoma.[29] More recently, Tyro3, along with several other RTKs, was shown to be highly activated across a broad spectrum of primary melanoma tissues and cell lines regardless of BRAF/NRAS mutational status.[30] High levels of Tyro3 and Axl expression have also been correlated with thyroid cancer.[31]

Here, we describe our efforts to characterize Gas6−Tyro3 interactions both biochemically and *in vitro* in melanoma cell lines. We evaluated Tyro3 expression across multiple melanoma tumor cell lines and demonstrated a strong Tyro3 dependence for tumor cell survival using short hairpin RNA-mediated Tyro3 knockdown. We also generated soluble and monomeric human Tyro3 extracellular domain and human Gas6 proteins to quantify the binding properties of the molecules because previous efforts to characterize the interactions of Gas6 and soluble TAM receptor constructs were performed mainly using Fc fusion proteins, which complicates quantitative affinity determinations.[3,32] A panel of mAbs with varying epitopes across the Tyro3 extracellular domain was generated. Biochemical and *in vitro* cell signaling experiments were performed to evaluate the potential role of Tyro3 as a survival receptor in melanoma and to assess the activities of these novel mAbs and associate them broadly with their various epitopes.

MATERIALS AND METHODS

Soluble Receptor and Ligand Reagents. hTyro3-ECD (hTyro3 signal with residues 1−388-Flag-10His) and hTyro3-Ig (hTyro3 signal with residues 1−222-Flag-10His) were subcloned from SC108283 (OriGene Technologies) and inserted into an in-house vector, PV90IRES, for mammalian expression. The PV90 vector was modified to express DHFR following an EMCV IRES linked to hTyro3. Expression of the soluble hTyro3 proteins in CHO was performed as described previously.[33] Human Gas6 (hGas6) and mouse Gas6 (mGas6) were purchased from R&D Systems. An in-house version of hGas6 was also generated, which behaved like the R&D Systems material in our assays. Human PS was purchased from HaemTech.

The soluble hTyro3 proteins were extracted from CHO supernatants by batch incubation with Ni^{2+}-NTA agarose beads (Qiagen). The beads were collected and washed with PBS and 20 mM imidazole. The hTyro3 proteins were eluted using PBS and 300 mM imidazole, dialyzed against 10 mM acetate (pH 5.0), and applied to a cation exchange column (SP Sepharose FF, GE Healthcare) equilibrated in the same buffer using an AKTA Explorer (GE Healthcare). The hTyro3 proteins were eluted from the column using a NaCl salt gradient from 0 to 500 mM. A small amount (~10−20%) of aggregated (trimeric) material was apparent in the hTyro3-ECD material after SP Sepharose purification. This material was separated from the monomeric hTyro3-ECD protein using a preparative SEC step (Superdex 200, GE Healthcare). The hTyro3-ECD and hTyro3-Ig proteins were concentrated using Amicon Ultra-15 centrifugal filter units (Millipore), dialyzed into PBS (Irvine Scientific), aliquoted, and stored at −70 °C. The hGas6 protein from R&D Systems was dialyzed against PBS supplemented with 2 mM $CaCl_2$ prior to being aliquoted and stored. In-house hGas6 was purified as described for PS,[34] except 2 mM $CaCl_2$ was added in every step and a final preparative SEC step (Superdex 200, GE Healthcare) was added to remove additional impurities and nonmonomeric material.

Anti-Tyro3 mAb Generation. A group of 6-week-old female BALB/c mice were initially immunized with 10 μg of hTyro3-ECD that was premixed with complete Freund's adjuvant. Reimmunization was performed with 10 μg of hTyro33-ECD in incomplete Freund's adjuvant. In total, animals were immunized three times, biweekly. Mouse serum was collected 1 week after the last immunization, and the antibody responses in the immune sera were evaluated by an enzyme-linked immunosorbent assay (ELISA) described below. The mouse chosen for hybridoma preparation received one additional boost of 10 μg of hTyro3-ECD 3 days prior to the cell fusion.

Splenocytes from a BALB/c mouse immunized with hTyro3-ECD were fused with mouse myeloma cells SP2/0 (American Type Culture Collection) at a 4:1 ratio using 50% polyethylene glycol (molecular mass of 1500 Da; Roche Diagnostic Systems). After fusion, cells were seeded and cultured in 96-well plates at a density of 1×10^5 cells/well in Dulbecco's modified Eagle's medium (DMEM)-F12 selection medium containing 20% fetal bovine serum (FBS), 2 mM L-glutamine, 100 units/mL penicillin, 100 μg/mL streptomycin, 10 mM HEPES, and 1× hypoxanthineaminopterin-thymidine (HAT)

dx.doi.org/10.1021/bi301588c | *Biochemistry* 2013, 52, 3102−3118

(Sigma). Hybridoma supernatants were screened for binding by an ELISA using hTyro3-ECD. Briefly, 96-well NUNC plates (Thermo Scientific) were coated with 1 μg/mL hTyro3-ECD and incubated overnight at 4 °C. After the sample had been washed and blocked with PBS containing 1% BSA and 0.05% Tween 20, 100 μL of hybridoma supernatant samples was added and incubated for 1 h at room temperature. The plates were washed, and the bound anti-Tyro3 antibodies were detected using horseradish peroxidase (HRP)-conjugated goat anti-mouse IgG (Pierce), followed by incubation with the substrate TMB (Thermo Scientific) for color development. Absorbance values were determined at 450 nm in a spectrophotometer. Selected hybridomas were subcloned via limiting dilution.

Analytical Size Exclusion Chromatography (SEC) and In-Line Static Light Scattering (SLS). The oligomeric states of hTyro3-ECD (monomer and trimer), hTyro3-Ig, and hGas6 were assessed using analytical SEC with in-line static light scattering. For each sample, 30 μg of hTyro3-ECD or -Ig or 50 μg of hGas6 (with or without Ca^{2+}) was injected onto a Biosep-SEC-S3000 analytical SEC—high-performance liquid chromatography (HPLC) (7.8 mm × 300 mm) column (Phenomenex) equilibrated in 10 mM phosphate, 150 mM NaCl, and 0.02% NaN_3 (pH 6.8) using an Agilent 1100 HPLC system. The hGas6 protein in the absence of Ca^{2+} was prepared by adding EDTA to a final concentration of 10 mM from a 1 M stock to the hGas6 stock solution followed by exhaustive dialysis in PBS (Irvine Scientific). Light scattering data for material eluted from the SEC column were collected using a mini-DAWN static light scattering detector coupled to an in-line refractive index meter (Wyatt Technologies). UV data were analyzed using HPCHEM (Agilent). Molecular masses of the proteins were determined by their static light scattering profiles using ASTRA V (Wyatt Technologies).

Circular Dichroism Spectroscopy (CD) and Differential Scanning Calorimetry (DSC). CD spectra were collected on an Applied Photophysics ChirascanPlus spectrapolarimeter. Scans were collected from 250 to 195 nm every 1 °C from 25 to 105 °C. Data were averaged for 0.7 s at each wavelength using a bandwidth of 1 nm. A 0.5 mm quartz cell supplied by the manufacturer was used for collection. For hGas6, the apoprotein, calcium was extracted from hGas6 by adding 4 mM EDTA. Holo- and apo-hGas6 samples were dialyzed against 4 mM Tris and 75 mM NaF with and without 2 mM $CaCl_2$, respectively.

DSC scans were performed using an automated capillary DSC instrument (capDSC, MicroCal, LLC). Receptor and ligand protein solutions and reference (buffer) solutions were sampled automatically from 96-well plates using the robotic attachment. Prior to each protein scan, two buffer scans were performed to define the baseline for subtraction. All 96-well plates containing protein were stored within the instrument at 6 °C. Each sample was diluted to 0.5 mg/mL in PBS (with or without 2 mM $CaCl_2$ for hGas6). Scans were performed from 10 to 95 °C at a rate of 2 °C/min using the low feedback mode. Scans were analyzed using the Origin software supplied by the manufacturer. Subsequent to the subtraction of reference baseline scans, non-zero protein scan baselines were corrected using a third-order polynomial. The unfolding parameters for each protein were deconvoluted using the multipeak fitting routine within the software assuming non-two-state unfolding behavior.

Surface Plasmon Resonance (SPR). All SPR experiments were performed on a Biacore 3000 instrument (GE Healthcare). The anti-His tag mouse mAb (PENTA-His, Qiagen) was immobilized to 10000 resonance units onto a research grade CM5 sensorchip at 20 μg/mL in 10 mM acetate buffer pH 4.0() using the standard amine coupling protocols provided by the manufacturer (GE Healthcare). Next, 10 μL of in-house hTyro3-ECD (monomer) was injected onto the sensorchip surface at a rate of 2 μL/min at 40 nM and captured via its histidine tag. The flow rate was increased to 20 μL/min, and 100 μL of hGas6 (between 4 μM and 4 nM) was injected over the Tyro3-ECD surface. The buffer was either HBS-P (GE Healthcare) or HBS-P supplemented with 2 mM $CaCl_2$. The flow rate was increased to 60 μL/min, and the surface was reliably regenerated using 2 × 5 μL injections of 0.1 M glycine (pH 2.0). The curves were double referenced by subtracting sensorgrams from a CM5 surface lacking the PENTA-His mAb followed by subtracting a sensorgram with 40 nM hTyro3-ECD (monomer) followed by an HBS-P (with or without 2 mM $CaCl_2$) injection. Provided the hTyro3-ECD and hTyro3-Ig proteins were 100% active, the maximal response in resonance units (R_{max}) expected for hGas6 was

$$R_{max}\text{hGas6} = \text{MW}_{\text{hTyro3}}/(\text{MW}_{\text{hGas6}} \times R_{\text{Tyro3}})$$

where $\text{MW}_{\text{hTyro3}}$ is the molecular mass of the hTyro3-ECD (44 kDa) or hTyro3-Ig (26 kDa) construct, MW_{hGas6} is the molecular mass of hGas6 (72 kDa), and R_{Tyro3} is the response in resonance units generated by the capture of each hTyro3 construct using the PENTA-His mAb. R_{hGas6} was plotted and fit to the steady-state equilibrium affinity equation provided by the manufacturer (GE Healthcare):

$$R_{\text{hGas6}} = (R_{max}\text{hGas6} \times C)/(K_D + C)$$

where C is the concentration of hGas6 titrated onto the hTyro3-captured sensorchip surface.

mAb cross-blocking was assessed using the same PENTA-His sensorchip surface. A triple-injection series starting with 40 nM hTyro3-ECD (monomer) was followed by back-to-back injections of 100 nM mAb A and mAb B. The flow rates were maintained at 20 μL/min, and the volume of each injection was 80 μL.

TAMR/Anti-Tyro3 mAb ELISAs. Each of the TAMR proteins [hTyro3-ECD (monomer), hTyro3-Ig, mTyro3-Fc, hAxl-Fc, and hMer-Fc] was biotinylated using the EZ-Link Sulfo-NHS-LC-Biotin kit (Thermo Scientific) using the protocols provided by the manufacturer and dialyzed exhaustively against PBS to remove unreacted material. Each receptor was added (4 μg/well) to Thermo StrepMax streptavidin precoated plates overnight at 4 °C. To investigate the ability of the anti-Tyro3 mAbs [raised against hTyro3-ECD (monomer)] to bind each of the receptor constructs, each mAb was serially titrated (1:3 dilutions) at starting concentrations between 1 μM and 200 nM across the plates (11 wells). Proteins were incubated on the plates for 1 h at room temperature (RT) and then washed five times with distilled deionized (DDI) water. The bound mAbs were detected using an HRP-labeled anti-mouse IgG-Fc polyclonal mixture (1:1000 dilution; Jackson Laboratories). After incubation for 1 h at RT, the plates were washed five times with DDI water followed by the addition of 100 μL of TMB substrate (KPL) per well. Following a short period of incubation (generally 2—10 min), the reaction was stopped by the addition of 1% phosphoric acid

(100 μL/well) and the absorbance at 450 nm was read using a SpectraMax UV plate reader.

Gas6/TAMR ELISAs. Human Gas6 (R&D Systems) was biotinylated in a PBS/2 mM $CaCl_2$ buffer using the EZ-Link Sulfo-NHS-LC-Biotin kit (Thermo Scientific) using the protocols provided and dialyzed exhaustively in the same buffer to remove any unreacted material. Biotinylated Gas6 was added at a concentration of 4 μg/mL (100 mL/well) to Thermo StrepMax streptavidin precoated 96-well plates overnight at 4 °C. The plates were washed five times with PBS and 2 mM Ca^{2+} followed by the addition of in-house hTyro3-ECD (monomer), hTyro3-ECD (trimer), or hTyro3-Ig or commercial hTyro3-Fc, hAxl-Fc, or hMer-Fc (100 μL/well). The soluble TAMR reagents were incubated on the plates for 1 h at RT. Typically, serial dilutions (1:3) were made across the plates starting at concentrations between 2 μM and 500 nM. The plates were then washed five times with PBS and 2 mM Ca^{2+} followed by the addition of mouse anti-Flag HRP (1:1000 dilution from a 250 μg/mL stock; Sigma) for the Flag-labeled in-house reagents or goat anti-human IgG-Fc-HRP (1:1000 dilution from a 0.5 mg/mL stock; Jackson Laboratories) for the commercial TAMR-Fc reagents. The plates were washed, and HRP activity was detected as described above.

To investigate the ability of the unlabeled receptors, ligands, and monoclonal antibodies to block the interaction between biotinylated hGas6 and hTyro3-ECD-Flag, the Tyro3-ECD-Flag reagent (50 nM for the monomer and 5 nM for the trimer) was co-incubated on the plate with various concentrations of the unlabeled reagents [1:3 serial dilutions starting between 4 μM (PS) and 200 nM (mAbs)] during the biotin-hGas6/hTyro3-ECD-Flag (second) binding step of the ELISA protocol.

Cell Growth. All human melanoma cell lines were purchased from American Type Culture Collection (ATCC) and grown in the indicated medium according to standard BL2 tissue culture conditions.

Lentivirus Production. A scrambled (SCR) and four TYRO3 short hairpins (shRNA), TRCN0000002178 (sh-1), TRCN0000002179 (sh-2), TRCN0000002180 (sh-3), and TRCN0000002181 (sh-4), used in this study are part of the TRC (The RNAi Consortium) collection. TYRO3 hairpins sh-2 and sh-4 were initially identified in a kinase-requirement screen across various cell lines.[26,35] Lentiviruses expressing these shRNAs were produced as previously described.[36,37] Virus was produced in six-well plates to generate the virus levels required for the experiments. Briefly, 293T packaging cells (ATCC) were seeded in DMEM containing 10% FBS at a density of 1.5 million cells per well 24 h prior to transfection with packaging plasmids and specific shRNA. The following day after a fresh change of medium, cells in each well were transfected with 1250 ng of lentiviral vector, 1250 ng of a gag-pol-rev expression plasmid, and 250 ng of a VSVG expression plasmid, using TransIT-LT1 transfection reagent according to the manufacturer's suggestions (Mirus Bio). Transfection mixtures were added to cells, centrifuged at 2250 rpm for 30 min, and held at 37 °C and 5% CO_2. Eight hours post-transfection, medium was replaced with DMEM containing 25% FBS. Supernatants were collected and pooled 48 and 60 h post-transfection. Supernatants with shRNA-containing lentivirus particles were clarified by centrifugation, aliquoted, and stored at −80 °C until they were required for transduction into the different melanoma cancer cell lines. Plasmid DNA for transfection was prepared using the Qiagen Midi-Prep Kit.

Ninety-Six-Well Transductions. Cells were cultured in appropriate medium designated by ATCC, washed, trypsinized, and seeded at a density of 2000 cells per well in 96-well plates (Corning Life Science) using a Sciclone robot (Caliper Life Science) in a final volume of 100 μL. Just prior to infection (~24 h postseeding), a 10× solution of Polybrene was added to the cells to a final concentration of 8 μg/mL. Lentiviruses expressing scrambled or Tyro3-specific shRNA were thawed, and serial dilutions were made in 96-well plates (Axygen) prior to infection; a constant 10 μL of virus was added per well using the Sciclone robot for a final volume of 120 μL per well. Cells were centrifuged at 2250 rpm for 30 min and held at 37 °C and 5% CO_2. A complete change of medium was made 12−16 h postinfection to remove Polybrene. A second change of medium was made 24 h prior to assessing viability using an Alamar Blue assay. Overall, the cells were grown for 7 days prior to the assessment of their viability. A 50× stock solution (150 mg/L) of Alamar Blue in PBS was diluted to a 10× working solution in an appropriate medium just prior to use. Using the Sciclone Robot (Caliper Life Science), 10 μL was added to each well and incubated at 37 °C for 2 h. The fluorescence was read using a Perkin-Elmer EnVision plate reader set to an excitation wavelength between 540 and 570 nm and an emission wavelength of 595 nm. The percent normalized cell death was calculated using the expression 100 − [(viability of TYRO3 shRNA)/(viability of scrambled shRNA)] × 100.

Flow Cytometry. ShRNA-transduced cells were washed, trypsinized, resuspended in medium between 72 and 96 h postinfection, and evaluated for Tyro3, Axl, and Mer expression. Cells were incubated for 30 min on ice with the following goat polyclonal primary mAbs at 10 μg/mL: anti-human Tyro3 AF859, anti-human Axl AF154, and anti-human Mer AF891 (all from R&D Systems). After the cells had been washed with PBS with 0.5% BSA, secondary detection was performed for 30 min on ice using polyclonal donkey anti-goat IgG Phycoerythrin F0107 (R&D Systems). After the samples had been washed, fluorescence measurements were performed, and data from 10000 single-cell events were collected using a standard FACScalibur flow cytometer (Immunocytometry Systems, Becton Dickinson). Data were analyzed using Flow Jo (Treestar).

mRNA Analyses in Normal and Malignant Skin Tissues. The Gene Logic ASCENTA database was used to examine the expression of TYRO3 (211432_s_at), AXL (202686_s_at), and MER (206028_s_at) in various skin samples. For each gene, only the probe set with the most robust expression values was considered. Data in the ASCENTA database were generated on the Affymetrix HG-U133A GeneChip.

mAb-Dependent Effects on Akt Phosphorylation in Melanoma Cell Lines. Cells were plated in serum-containing growth medium at a density of 6×10^5 cells/well of a six-well plate and allowed to attach overnight at 5% CO_2 and 37 °C. Cells were serum starved in medium containing no FBS overnight. Cells were treated with each mAb (30 μg/mL) diluted in serum-free medium for 30 min at 37 °C (0.5 mL/well). Recombinant mGas6 or serum was diluted to 2 times the final concentration in serum-free medium, and 0.5 mL was added per well and incubated for 30 min at 37 °C and 5% CO_2. Plates were placed on ice and washed once with ice-cold PBS, and 70 μL of complete lysis buffer [20 mM Tris-HCl (pH 7.4), 150 mM NaCl, 1 mM EDTA, 1 mM EGTA, 1 mM NaF, 20

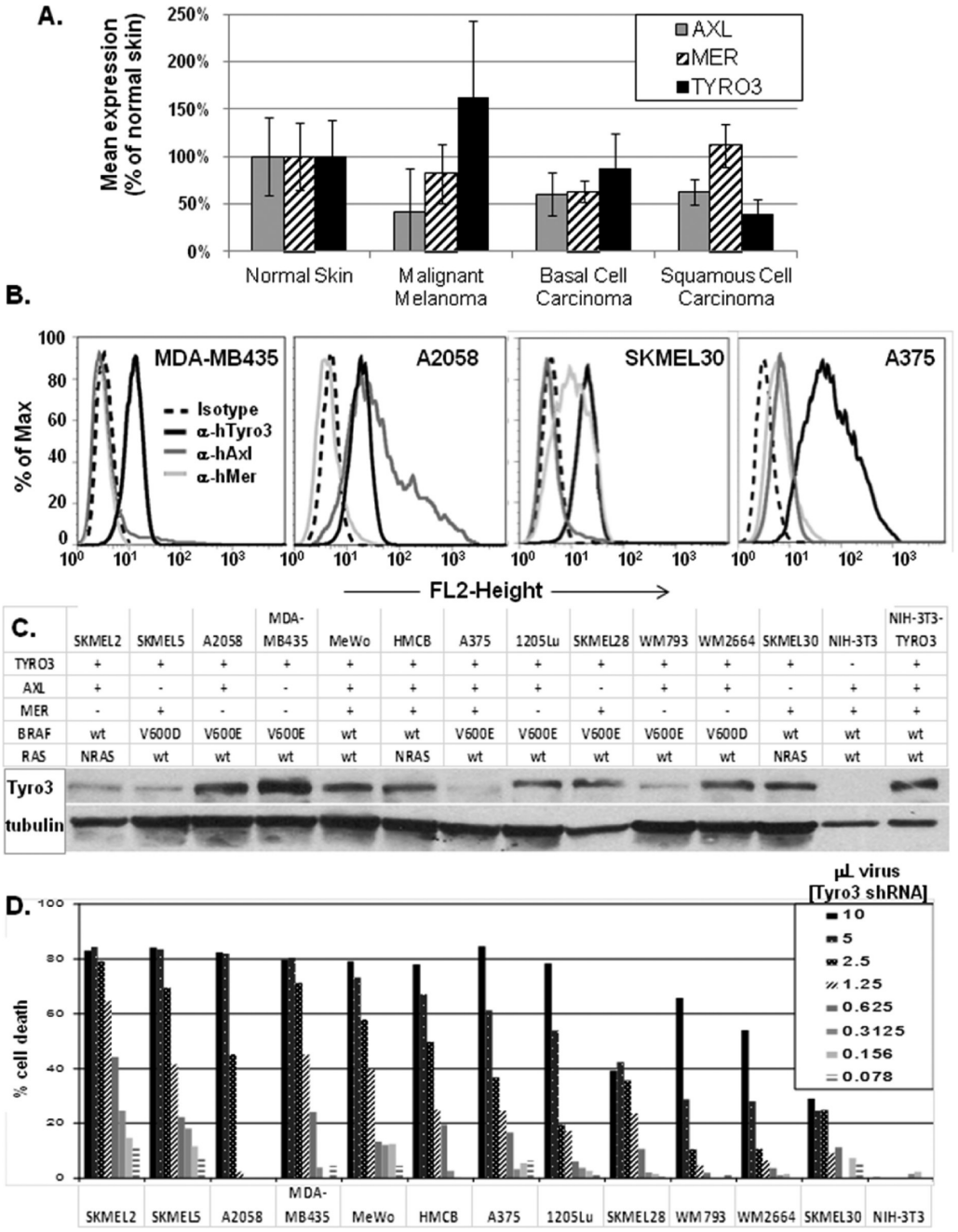

Figure 1. Tyro3 is expressed in primary melanoma and melanoma cell lines. (A) Analysis of Tyro3 mRNA levels in normal skin, malignant melanoma, basal cell carcinoma, and squamous cell carcinoma of the skin from the Gene Logic ASCENTA library as expressed as the mean intensity as the percent of normal skin expression levels. (B) FACS analysis of four melanoma cell lines with different TAMR co-expression patterns. (C) Summary of Tyro3 protein expression in a panel of melanoma cell lines. NIH-3T3 and TYRO3-transfected NIH-3T3 were used as controls. The presence (+) and absence (−) of Tyro3, Axl, and Mer proteins by FACS (compared to a negative isotype control) are indicated. The presence of Tyro3 based on Western blot analysis is also shown. Also listed is the BRAF and NRAS mutational status as determined by sequencing (in-house, Cosmic, Broad Cell Line Encyclopedia). (D) Cell viability of various melanoma tumor cell lines after transduction with a range of TYRO3 sh-2 viral supernatant volumes as indicated.

mM $Na_4P_2O_7$, 2 mM Na_4VO_4, 1% Triton X-100, 0.1% SDS containing 1× complete protease inhibitor cocktail (Roche), 1:100 dilutions of phosphatase inhibitor cocktails I and II (Sigma-Aldrich), and 2 mM PMSF] was added per well. Cells were scraped and transferred to Eppendorf tubes on ice for 30 min. Cellular debris was removed by centrifugation at 14K rpm for 20 min at 4 °C, and cleared lysates (supernants) were saved for assays. The total protein was assessed by the BCA assay (ThermoScientific), and samples were diluted for Western blot analyses.

Western Blots. For Western blots for the detection of Tyro3, cells were lysed using complete lysis buffer (described above) containing 1× complete protease inhibitor cocktail (Roche). Total protein (50 μg) was diluted into loading dye, boiled for 5 min, and applied to a NuPAGE 4 to 20% Tris glycine gel. Proteins were transferred to nitrocellulose using the iBlot dry blotting system (Invitrogen) and blocked for 1 h in

dx.doi.org/10.1021/bi301588c | *Biochemistry* 2013, 52, 3102−3118

TBS containing 0.1% Tween 20 (TBST) and 5% nonfat dry milk. Washing was performed with TBST. Tyro3 was detected after a 1 h incubation with mouse anti-hTyro3 mAb859 (R&D Systems, 1:500 dilution), followed by a 1 h incubation with goat anti-mouse IgG HRP (Jackson Laboratories, 1:1000 dilution). Blots were washed and imaged on film with SuperSignal West Dura Extended Duration Substrate (Thermo Scientific).

For cell signaling Western blots, 20−30 μg of total protein was diluted in reducing loading dye, boiled, and applied to a 10% Tris-HCl polyacrylamide gel (Bio-Rad). Proteins were transferred to nitrocellulose using the IBlot dry blotting system (Invitrogen) and blocked for 1 h in Odyssey Blocking Buffer (Li-Cor Biosciences) or TBST and 5% nonfat dry milk. Primary antibodies from Cell Signaling Technology were used at 1:1000 dilutions in blocking buffer and 0.1% Tween20 overnight at 4 °C with rocking [p44/42 MAPK #4696, phospho-p44/42 MAPK Thr202/Tyr204 #4370, phosphoAKT (Ser473) #4058, total AKT #2920, anti-α-tubulin (clone DM-1A, Sigma-Aldrich)]. After antibody incubation, blots were washed with wash buffer (TBST) for 3 × 10 min and then incubated with 1:5000 to 1:15000 dilutions of Dylight 800 goat anti-rabbit IgG (#35571) and Dylight 680 goat anti-mouse IgG (#35518, ThermoScientific) in Odyssey Blocking Buffer and 0.1% Tween 20 for 1 h at room temperature. Blots were washed briefly in TBST, rinsed in PBS, and imaged on the Odyssey Infrared Imaging System (Li-Cor).

Immunoprecipitation of Phospho-Tyro3. Cells were plated at a subconfluent density in multiple T-150 flasks and allowed to attach overnight. Cells were then serum starved in medium containing no FBS overnight. Cells were then treated with ligand (mGAS6) or antibody at the indicated doses and incubated at 37 °C for 30 min. Flasks were placed on ice, and cells were washed briefly with ice-cold PBS. Cells were scraped and collected, pelleted, and lysed with complete lysis buffer. Cell lysates were prepared as previously described. One to two milligrams of total protein was transferred to a clean Eppendorf tube, and anti-Tyro3 antibody (6 μg of sc-1095, Santa Cruz Biotechnology) and 100 μL of Protein G-Agarose (#20398, Thermo Scientific) were added directly to the lysate and incubated while being rocked at 4 °C overnight. Agarose was pelleted at 5000 rpm for 10 min and washed twice with lysis buffer. Ten microliters of reducing loading dye and 20−30 μL of lysis buffer were added to agarose, pelleted, mixed gently with a pipet tip, and boiled for 10 min. Agarose was pelleted, and the eluant was separated on a 7.5% Tris-HCl Criterion gel (Bio-Rad) and immunoblotted to nitrocellose. Membranes were blocked in TBST and 5% nonfat dry milk for 1 h at room temperature and then incubated with primary antibodies. The anti-phosphotyrosine 4G10 mouse monoclonal antibody (Millipore) was used at a 1:1000 dilution in TBST and 5% nonfat dry milk overnight at 4 °C with rocking. Total Tyro3 was detected with MAB859 (R&D Systems) or Epitomics anti-Tyro3 #3218-1 RabMab at a 1:1000 dilution in TBST and 5% nonfat dry milk overnight. Membranes were then washed for 3 × 10 min in TBST. Secondary antibodies (Bio-Rad goat anti-rabbit HRP #170-6515 or goat anti-mouse HRP #170-6516) were diluted in TBST and 5% nonfat dry milk ata 1:4000 (rb) or 1:10000 (ms) dilution and incubated on membranes for 1 h at room temperature. Blots were washed and imaged on film with SuperSignal West Dura Extended Duration Substrate (Thermo Scientific).

Cleaved PARP and Cleaved Caspase-3 ELISA. Cells treated with lentivirus-delivered shRNA were collected and lysed in complete lysis buffer and stored at −20 °C. Twenty micrograms of total protein diluted in 0.5% Block B (provided) was added per well to the MSD Multiplex Apoptosis Panel ELISA plate (Meso Scale Discovery) in duplicate and incubated overnight at 4 °C. The ELISA was finished as described by the manufacturer and analyzed on the SECTOR Imager 6000 reader.

RESULTS

Relative Expression of Tyro3 in Human Tissues and Melanoma Tumor Samples. The relative levels of TYRO3, AXL, and MER mRNA in various normal and tumor tissues within the Gene Logic ASCENTA database, which contains gene expression data from annotated human tissue samples, were analyzed. Transcript expression profiles of the TAMR family indicate large nonoverlapping patterns of expression in both normal and malignant tissue sets (Figure S1A,B of the Supporting Information). Consistent with literature reports, normal Tyro3 expression is primarily restricted to the brain, testis, and ovary. Axl is abundantly expressed in a majority of tissues, whereas Mer expression seems to be restricted to lymphocyte/monocyte-derived cells. Strikingly, in malignancies, Tyro3 expression is highly restricted with overexpression noted in melanoma, lung, and ovarian cancer tissues, whereas Axl is commonly overexpressed in tumor cells from tissue types that normally express the RTK, such as colon, pancreas, lung, breast, ovary, stomach, skin, and prostate.

Next, we focused our evaluation of TAMR expression on normal and cancerous skin tissues. Normal skin samples were compared with aberrant skin tissue samples, including malignant melanoma, basal cell carcinoma, and squamous cell carcinoma (Figure 1A). According to the eNorthern data derived from the ASCENTA skin sample set, TYRO3 was overexpressed ($p < 0.001$) in malignant melanoma over normal skin, but not in squamous cell carcinoma or basal cell carcinoma (Figure 1A). No clear deviations from normal skin were observed for MER in any of the aberrant tissue types, whereas in all the aberrant skin samples, but most notably in melanoma, the AXL message was significantly weaker. Of note, while the eNorthern data derived from the ASCENTA skin data set were based on inclusion of all samples, TYRO3 was labeled "present" in 57% of the malignant melanoma samples and it was called present in only 6% of the normal skin cell samples. We independently investigated TYRO3, AXL, and MER mRNA levels in normal skin and melanoma tumor cell cDNA samples from primary melanoma patients (provided by OriGene) using quantitative polymerase chain reaction (PCR). In agreement with the data obtained from ASCENTA (Figure 1A and Figure S1C of the Supporting Information), TYRO3 was generally at least 2-fold upregulated compared with that in normal skin, while AXL was expressed at significantly lower levels in tumor tissues than in normal skin (Figure S1C of the Supporting Information). Again, no correlation was observed for MER.

Next, we examined Tyro3 protein expression in a panel of 12 melanoma tumor cell lines. Using flow cytometry, Tyro3 was found to be expressed in all cell lines tested (an in-house hTyro3-transfected NIH-3T3 fibroblast cell line was used as a control), whereas the sibling receptors Axl and Mer were variably co-expressed in the different lines (Figure 1B,C). For example, MDA-MB435 expressed only Tyro3, A2058 expressed

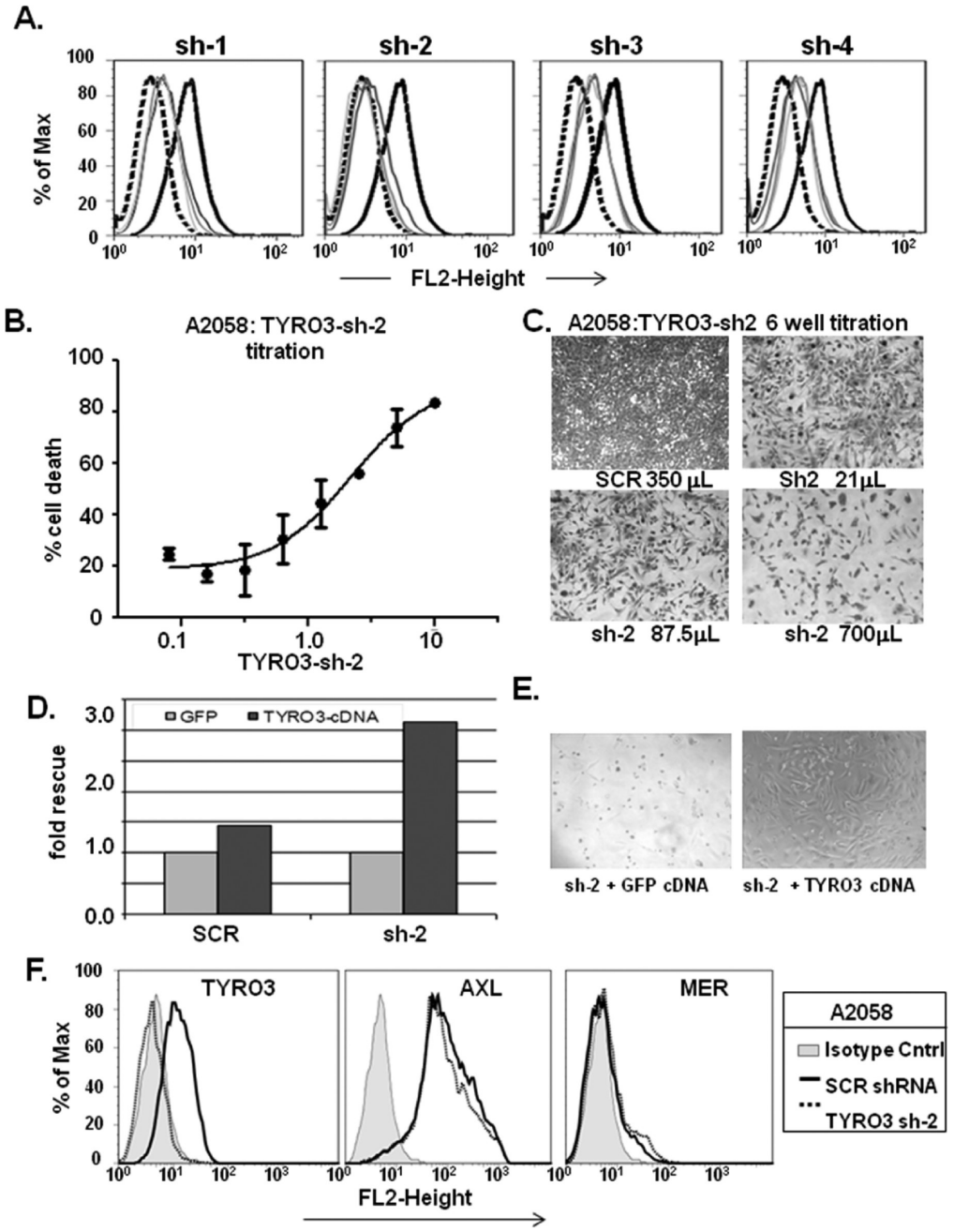

Figure 2. Selection of TYRO3 targeting shRNA and demonstration of TYRO3 selectivity. (A) TYRO3 knockdown in A2058 melanoma cells by different hairpins assessed by FACS: (solid black line) scrambled, i.e., TYRO3 expression control, (dotted line) IgG isotype control, and (increasingly gray lines) 21, 88, and 700 μL of virus, respectively. Only TYRO3 sh-2 leads to complete loss of Tyro3 protein (gray histograms). (B) Transduction with virus carrying TYRO3 sh-2 leads to a >80% loss of A2058 cell viability (measured by Alamar Blue) after 7 days in a viral dose–response assay. (C) Photomicrographs of A2058 cells treated with indicated TYRO3 sh-2 viral supernatants in a six-well scale-up experiment show growing losses of cell viability. (D) TYRO3 cDNA-mediated viability rescue in the A2058 melanoma cell line, as shown by Alamar Blue viability measurements, with sh-2 and scrambled virus effects expressed as fold over GFP control. (E) Photomicrographs of A2058 cells treated with TYRO3 sh-2 after transduction with GFP-cDNA (left) or TYRO3-cDNA (right). (F) TYRO3 sh-2 knocks down TYRO3 but has no effect on AXL or MER expression on A2058 cells (AXL, positive; MER, negative). This was also true in cell lines that expressed MER (data not shown).

both Tyro3 and Axl, and SKMEL30 expressed Tyro3 and Mer (Figure 1B,C). Tyro3 expression was also detected in all 12 melanoma cell lines using Western blots. Although the absolute presence of TYRO3 was correctly assessed by both methods, the relative levels of Tyro3 protein expression did not entirely correlate between the two methods (Figure 1C), and the reason for this disconnect is not clear.

Short Hairpin RNA (shRNA) Knockdown of Tyro3 in Melanoma Tumor Cell Lines. Initially, we compared the ability of four different TYRO3-specific shRNA hairpins to reduce Tyro3 protein levels on A2058 cells. TYRO3 sh-2 was the only hairpin to result in complete Tyro3 protein knockdown as measured by flow cytometry (Figure 2A). TYRO3 sh-2 transduction also corresponded with potent A2058 cell killing (Figure 2B,C). To confirm that the cell

dx.doi.org/10.1021/bi301588c | *Biochemistry* 2013, 52, 3102–3118

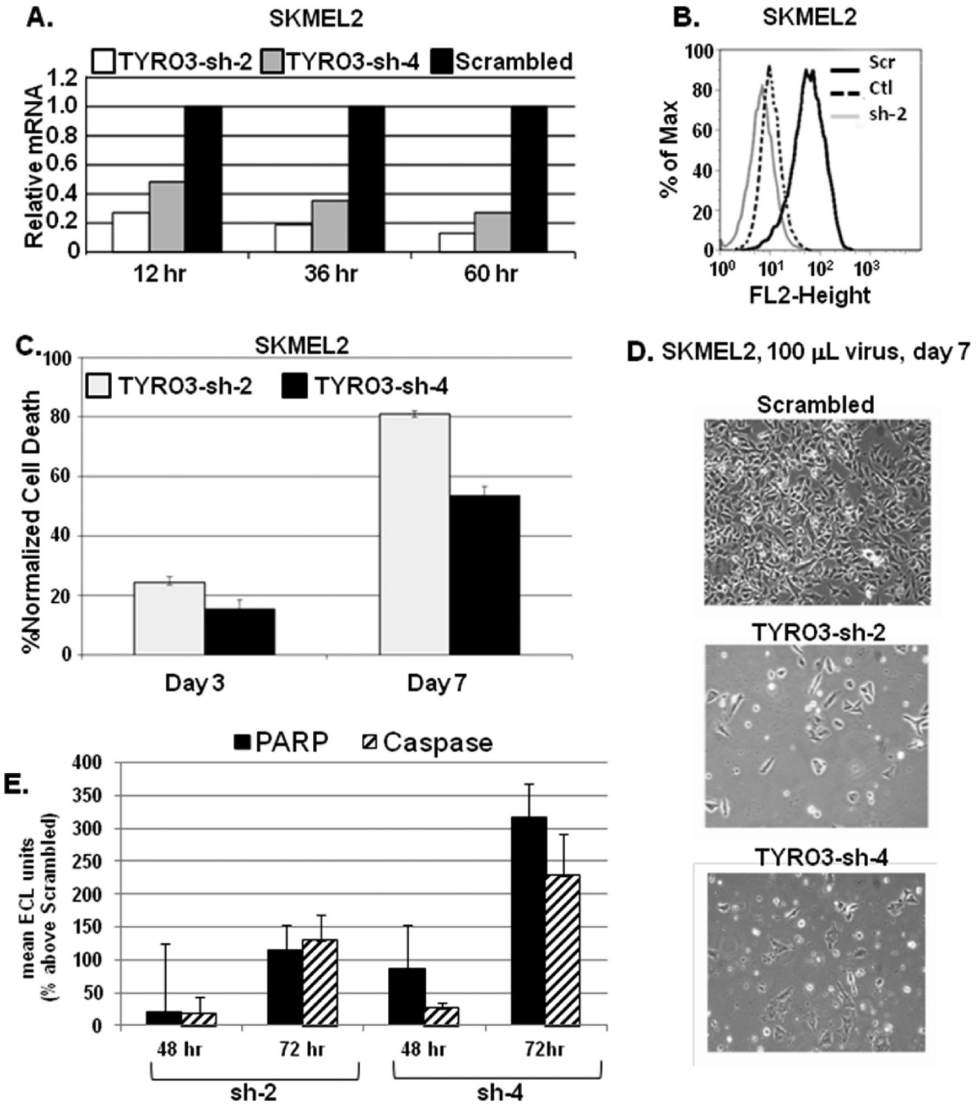

Figure 3. ShRNA knockdown of Tyro3 causes cell death by apoptosis in melanoma cell lines. Demonstration of specific Tyro3 knockdown by TYRO3-specific RNA hairpins TYRO3 sh-2 and TYRO3 sh-4 using reverse transcription PCR (A) and flow cytometric analyses (B) 3 days after transduction in the SKMEL-2 melanoma cell line. Scr indicates incubation with scrambled shRNA, and Ctl indicates a nonspecific primary IgG control during detection. (C) SKMEL-2 viability 3 and 7 days after transduction with TYRO3 sh-2 and TYRO3 sh-4 and (D) photomicrographs of the corresponding cell cultures on day 7 after treatment with TYRO3 or scrambled RNA hairpins. The percent normalized cell death was calculated as $100 - [(\text{hairpin signal})_{avg}/(\text{scrambled hairpin signal})_{avg}] \times 100$. (E) Increase in the level of cleaved PARP and cleaved caspase-3 after treatment for 48 and 72 h with TYRO3 sh-2 and TYRO3 sh-4. The increase in the level of PARP and caspase-3 cleavage (*Y*-axis) was calculated using a treatment of the MSD ECL data similar to that of the percent normalized cell death in panel C.

killing effect of TYRO3 sh-2 was specific to Tyro3 knockdown, A2058 cells were transduced with TYRO3 sh-2 then subsequently transfected with a TYRO3 cDNA expression construct not targeted by TYRO3 sh-2. The cDNA construct was able to rescue A2058 cells after Tyro3 knockdown with TYRO3 sh-2 (Figure 2D,E).

The 12 Tyro3-expressing melanoma lines described above were all transduced with TYRO3 sh-2 shRNA. The viability of the cell lines was assessed 7 days post dose titrating transductions with TYRO3 sh-2. Of the 12 cell lines, five cell lines were very sensitive to TYRO3 knockdown with a decrease in cell viability of ~80% (Figure 1D), six cell lines were moderately sensitive with a level of cell death between 40 and 80% after TYRO3 loss, and the one remaining cell line (SKMEL30) demonstrated ~20% cell death after transduction with the TYRO3 hairpin. Clearly, knockdown of Tyro3 had a negative impact on tumor cell survival. Flow cytometry was performed in parallel on cell lines treated with shRNA to confirm Tyro3 protein knockdown and to evaluate the presence of the other two TAMR proteins following TYRO3 gene knockdown. In general, 3 days post-transduction with TYRO3 sh-2 shRNA, Tyro3 expression was clearly suppressed as assessed by both mRNA detection and FACS (Figure 3A,B), with no effects on expression levels of Axl and Mer (Figure 2F). There was no correlation between relative Tyro3 levels as determined by FACS and sensitivity to Tyro3 knockdown. Co-expression of either Axl or Mer also had no apparent impact on cell viability, suggesting that loss of Tyro3 function could not be offset by the activity of other TAMRs (Figure 1C,D). Additionally, the BRAF and NRAS mutational status, as referenced in the COSMIC database and the Cancer Cell Line Encyclopedia (http://www.broadinstitute.org/cm3le/

dx.doi.org/10.1021/bi301588c | *Biochemistry* 2013, 52, 3102−3118

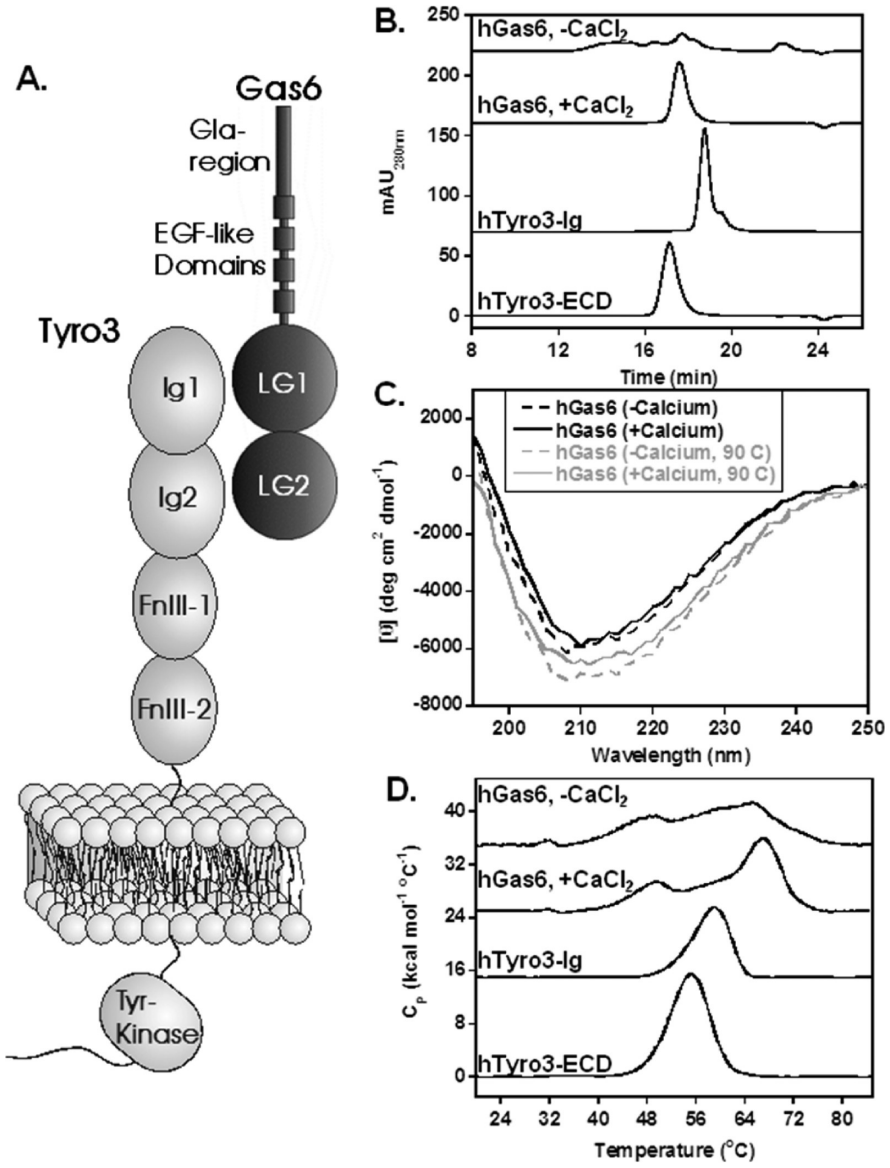

Figure 4. Biophysical characterization and activity of Tyro3 and Gas6 reagents. (A) Schematic diagram of the domain architecture of Tyro3 (and Axl/Mer) and Gas6. Tyro3's extracellular domain (ECD) comprises two Ig fold domains and two FnIII domains that lead into a transmembrane helix and a cytoplasmic tyrosine kinase domain. The N-terminus of Gas6 consists of several pairs of γ-carboxylated glutamate residues known as the Gla region. The Gla region is followed by four small EGF-like domains and two large laminin-like globular domains (LG) also known as sex hormone binding globulin domains. The LG domains of the ligand (particularly LG1) and Ig domains of the TAM receptors (particularly Ig1) are known to interact with one another. (B) Analytical size exclusion chromatography (bottom to top) of hTyro3-ECD, hTyro3-Ig, hGas6 (2 mM Ca^{2+}), and hGas6 (0 mM Ca^{2+}). (C) Far-UV CD spectra of 5.5 μM hGas6 in the presence and absence of 2 mM $CaCl_2$ at 30 and 90 °C. (D) DSC thermal unfolding curves of hTyro3-ECD, hTyro3-Ig, hGas6 (2 mM Ca^{2+}), and hGas6 (0 mM Ca^{2+}) (bottom to top, respectively).

home) and independently confirmed by the in-house Biogen Idec mutation sequence database, had no correlation with the observed results (Figure 1C,D). Finally, there was no correlation between the Tyro3 expression level and the sensitivity to shRNA knockdown, possibly because of co-expression of other growth factor receptors, other survival genes, or other (epi) genetic mechanisms specific to each melanoma cell line, which warrants additional future investigations of this phenomenon.

To determine whether the loss of cell viability resulting from the shRNA knockdown of Tyro3 occurred though apoptotic mechanisms, we searched for the presence of cleaved caspase-3 and PARP at different time points in the SKMEL2 model after shRNA lentivirus transduction. Efficient knockdown of TYRO3 mRNA and Tyro3 protein was confirmed by reverse transcription PCR and FACS, respectively (Figure 3A,B) and distinctly preceded the loss of viability that was evident on day 7 but not on day 3 (Figure 3C,D). The levels of cleaved PARP and caspase-3 were significant 72 h after Tyro3 knockdown (Figure 3E).

Characterization of Human Tyro3/Gas6 Protein Reagents. Two recombinant human Tyro3 proteins, one consisting of the entire extracellular domain (denoted hTyro3-ECD) and the other of the N-terminal Ig domains (denoted hTyro3-Ig), were produced using CHO cells and characterized extensively for their oligomeric-state, stability, and quantitative binding properties. A schematic diagram of the Tyro3 protein is provided in Figure 4A to help orient the reader. After

dx.doi.org/10.1021/bi301588c | *Biochemistry* 2013, 52, 3102−3118

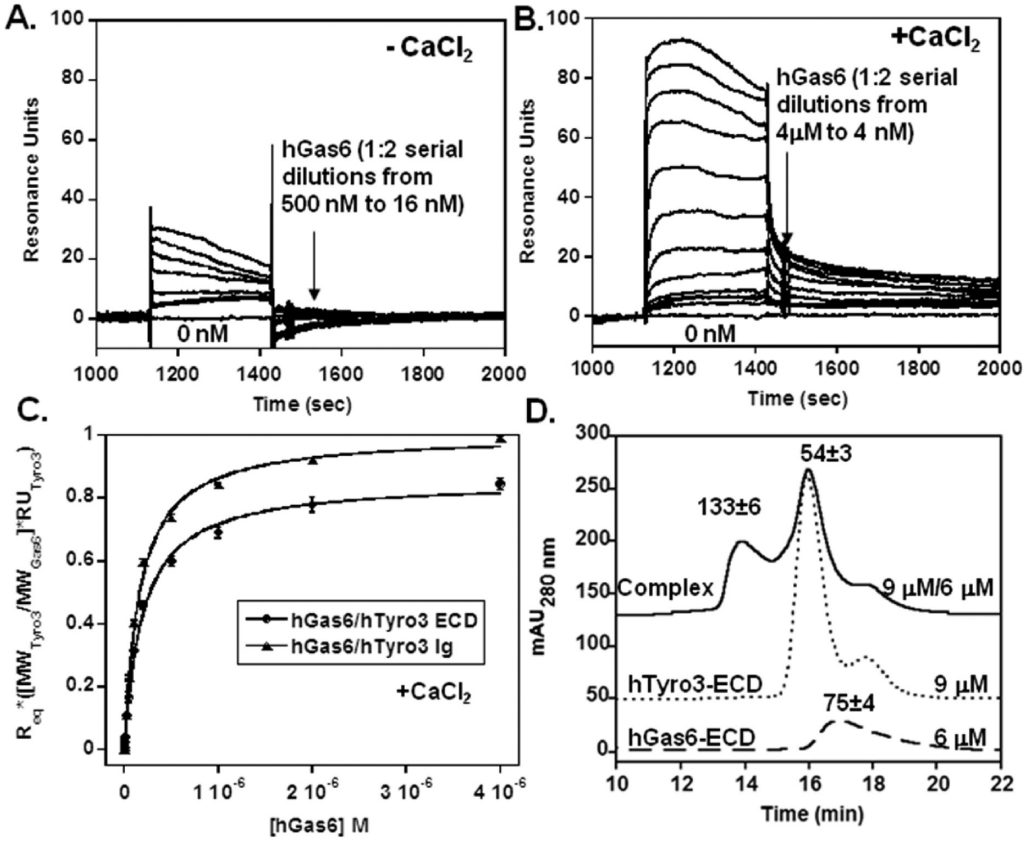

Figure 5. Equilibrium binding of hGas6 to hTyro3. Kinetic SPR curves of binding of hGas6 to surface-bound hTyro3-ECD in the (A) absence and (B) presence of 2 mM Ca^{2+}. (C) Steady-state equilibrium SPR binding curves for binding of monomeric hGas6 to monomeric hTyro3-ECD and hTyro3-Ig. (D) Analytical SEC with in-line static light scattering of hGas6 (40 μg), hTyro3-ECD (40 μg), and the complex at a hGas6:hTyro3-ECD ratio of 40 μg to 40 μg (6 μM to 9 μM). The running buffer consisted of 10 mM Tris (pH 8.0), 150 mM NaCl, and 2 mM $CaCl_2$. Small, calcium-dependent artifacts on the right side of all the SEC peaks (including an antibody reference sample) were apparent. The molecular masses of each SEC peak (determined by SLS) are listed above each peak.

purification, hTyro3-ECD and hTyro3-Ig were monomeric based on analytical SEC−SLS measurements (Figure 4B). The purified Tyro3 proteins were highly stable for >6 months at 4 °C with no changes in their oligomeric states.

We also generated recombinant human Gas6 (hGas6) from CHO cells (see Figure 4A for a schematic diagram). Without Ca^{2+} in the solution, the hGas6 protein aggregated and rapidly lost its activity (Figure 4B). Gas6 is known to bind Ca^{2+} ions in both the N-terminal Gla region and the LG domains. In the crystal structure of the Gas6 LG domains, there is a Ca^{2+} ion coordinated between the two LG domains.[38] If hGas6 is reconstituted in Ca^{2+} (or purified entirely in the presence of Ca^{2+}), the protein is stable and active for months at 4 °C in a monomeric state (Figure 4B). Monomeric Tyro3-ECD (~54 kDa based on SLS measurements) migrated significantly faster than hGas6 (~74 kDa by SLS) on the SEC column. In fact, Tyro3-ECD migrates at the same rate as control IgG proteins with a molecular mass of 150 kDa. This suggests the four-domain protein likely exists in an elongated structural conformation similar to that depicted in the schematic diagram in Figure 4A.

All three proteins, hTyro3-ECD, hTyro3-Ig, and hGas6 (in the presence of 2 mM $CaCl_2$), were well folded as determined by CD and DSC (Figure 4C,D). While the apparent structure of hGas6 is maintained in the presence and absence of Ca^{2+}, a clear difference in the thermal stability of hGas6 in the presence and absence of $CaCl_2$ was apparent based on both CD and DSC measurements (Figure 4C,D). Removal of Ca^{2+} led to an onset of unfolding at a 5 °C lower midpoint of temperature denaturation in our CD experiments (T_m = 57 and 62 °C in the absence and presence of Ca^{2+}, respectively). Removal of Ca^{2+} also decreased the cooperativity of unfolding of the largest transition in the hGas6 DSC unfolding profile with a decrease in the van't Hoff enthalpy of unfolding (ΔH_{VH}). Thus, Ca^{2+} suppresses the aggregation behavior of hGas6, and Ca^{2+} binding clearly stabilizes the protein.

Binding of hGas6 to hTyro3-ECD was investigated using SPR. The hGas6 protein was titrated onto sensorchip surfaces preloaded with hTyro3-ECD (monomer). In the absence of Ca^{2+}, only weak binding was observed (data not shown). However, in the presence of Ca^{2+}, a much clearer binding event that reached saturation near 2 μM hGas6 was evident (Figure 5A). Near identical binding could be achieved using hTyro3-Ig in place of hTyro3-ECD. Quantitative equilibrium binding constants (K_D values) were calculated using a steady-state affinity analysis (hGas6/hTyro3-ECD K_D = 190 ± 30 nM; hGas6/hTyro3-Ig K_D = 160 ± 30 nM) with a binding stoichiometry near 1:1 (Figure 5B). These K_D values suggest the affinity of Tyro3 for Gas6 is lower than previously reported (K_D between 0.04 and 10 nM).[3] Many previous studies utilized multimerized or IgG-Fc fusion proteins where avidity can increase the apparent affinity. Indeed, much stronger apparent binding was observed between hTyro3-Fc, hAxl-Fc, or hMer-Fc and surface-bound hGas6, but with multiexponential kinetics

dx.doi.org/10.1021/bi301588c | Biochemistry 2013, 52, 3102−3118

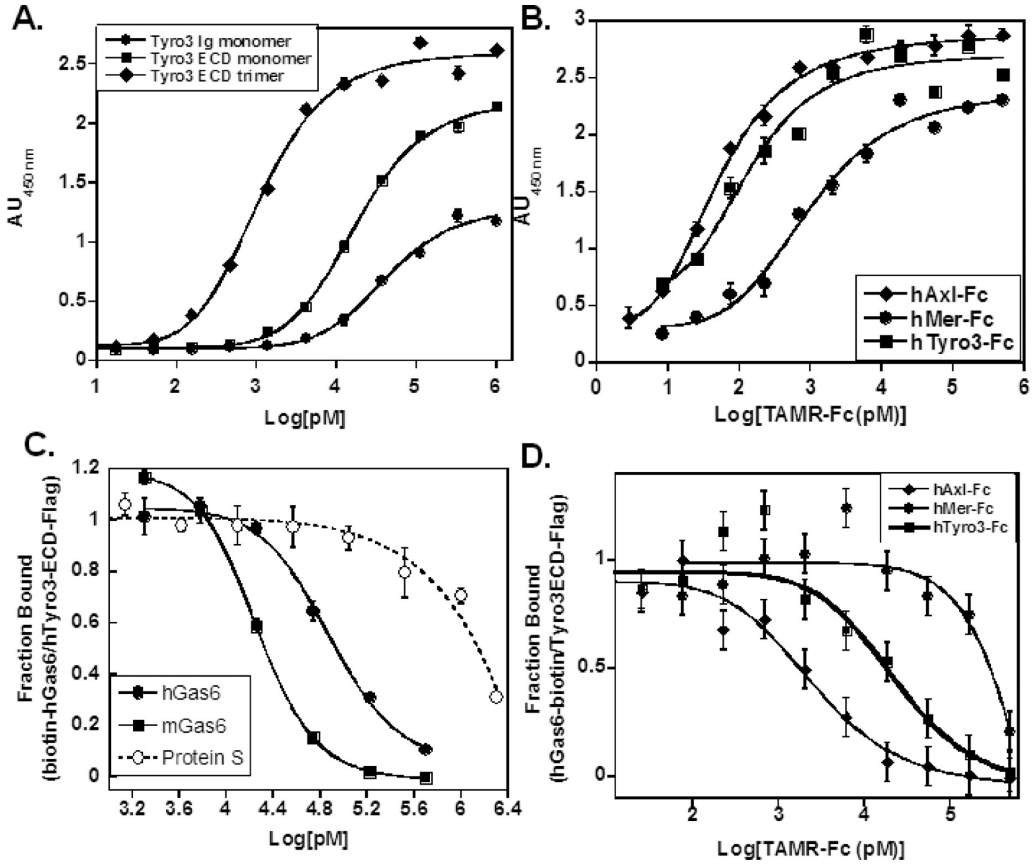

Figure 6. Direct ELISA and inhibitory ELISA measurements of the relative strengths of binding of Gas6 to Tyro3, Axl, and Mer. (A) Direct ELISA binding curves of monomeric hTyro3-ECD, hTyro3-Ig, and a trimeric version of hTyro3-ECD (purified as an ~15% fraction of the final preparative SEC step) binding to biotinylated hGas6. In-house Tyro3 proteins used to generate signals were detected using an engineered Flag tag. (B) Direct ELISA binding curves of hTyro3-Fc, hAxl-Fc, and hMer-Fc (all from R&D Systems) for binding to biotinylated hGas6. (C) Blocking of binding of hTyro3-ECD(-Flag) to biotinylated hGas6 by unlabeled mouse and human Gas6 and PS. (D) Blocking of binding of hTyro3-ECD(-Flag) to biotinylated hGas6 by hTyro3-Fc, hAxl-Fc, and hMer-Fc.

reflective of a strong avidity component. A rank ordering of apparent binding strengths of the TAMRs for hGas6 was similar to what has been reported previously (hAxl-Fc > hTyro3-Fc > Mer-Fc). SEC–SLS measurements were also utilized to evaluate the binding stoichiometry of the soluble hTyro3 proteins with respect to hGas6. Adding a 50% molar excess of hTyro3-ECD to hGas6 led to the appearance of a larger protein complex with a measured molecular mass (determined by SLS) of ~133 kDa, equivalent to a 1:1 binding stoichiometry (Figure 5C). A similar result was obtained pairing the smaller hTyro3-Ig with hGas6 with the appearance of an ~90 kDa protein complex in the SEC chromatogram (data not shown).

ELISA-Based Characterization of TAMR–Ligand Interactions. Further evaluation of the relative affinity of each of the TAMRs for Gas6 (and PS) was important for interpreting experimental results with mouse mAbs raised against hTyro3 (described below) and for utilizing the appropriate ligand or TAMR-Fc concentrations in cell-based assays. Therefore, all the TAMR proteins, Gas6, and PS were tested for their relative binding strengths in numerous ELISA-based protocols. First, in-house hTyro3-ECD monomer, hTyro3-ECD trimer (isolated during purification), and hTyro3-Ig proteins and the purchased hTyro3-Fc, hAxl-Fc, and hMer-Fc proteins were tested for their ability to bind hGas6 (Figure 6A,B). The avidity contribution of IgG-Fc fusion is clearly evident when comparing the hTyro3-Fc or Tyro3-ECD-trimer EC_{50} values to those obtained for monomeric hTyro3-ECD and hTyro3-Ig, whose EC_{50} values were approximately 100-fold lower (Table 1). The TAMR-Fc proteins all bound tightly to immobilized hGas6 with an apparent rank ordering consistent with the SPR results (Table 1) (Axl-Fc > Tyro3-Fc > Mer-Fc).

A competition ELISA was developed using hGas6 and the trimeric form of hTyro3-ECD generated during purification (to improve assay sensitivity). Both hGas6 and hPS could inhibit hTyro3-ECD from binding the plate (Figure 6C and Table 1). In agreement with published data,[3] the mouse Gas6 protein was significantly more potent (5-fold) than hGas6 at inhibiting the interaction, suggesting mGas6 has a higher affinity for hTyro3. These data influenced our decision to use mGas6 in the cell-based assays. This difference in affinity should be considered in preclinical or translational studies comparing the activities of the mouse and human TAMR signaling processes. The TAMR-Fc proteins all inhibited the interaction at IC_{50} values much lower than the EC_{50} values obtained using the direct ELISA where avidity was observed (Figure 6D and Table 1). The difference between the relative affinity of hAxl, hTyro3, and hMer for hGas6 is much more apparent in the competition (soluble) assay format. The IC_{50} values are reflective of the real affinity values of the TAMRs for hGas6 with the possible exception of hAxl-Fc, which reached the limit of the assay's ability to measure affinity.

dx.doi.org/10.1021/bi301588c | *Biochemistry* 2013, 52, 3102–3118

Table 1. TAMR−Ligand ELISA Binding and Blocking Behavior

hGas6 binding ELISA	EC_{50} (nM)
hTyro3 (monomer)	16 ± 4
hTyro3 (trimer)	1.0 ± 0.3
hTyro3-Ig domains	40 ± 10
hTyro3-Fc	0.13 ± 0.03
hAxl-Fc	0.05 ± 0.01
hMer-Fc	1.0 ± 0.3
hGas6−hTyro3 monomer blocking ELISA	IC_{50} (nM)
hGas6	80 ± 20
mGas6	16 ± 4
hPS	2500 ± 1000
hTyro3-Fc	3.6 ± 0.4
mTyro3-Fc	80 ± 100
hGas6−hTyro3 trimer blocking ELISA	IC_{50} (nM)
hGas6	100 ± 25
hPS	2500 ± 1500
hTyro3-Fc	25 ± 15
hAxl-Fc	2.5 ± 1.5
hMer-Fc	250 ± 150

Ligand-Induced Tyro3 Signaling. It has been reported that the TAMRs can signal through the PI3K/Akt pathway.[5] Therefore, we assessed ligand-induced Tyro3 phosphorylation and Akt phosphorylation. We utilized a melanoma cell line that endogenously expresses Tyro3, SKMEL2, and a hTYRO3-transfected NIH-3T3 cell line that expresses a high level of Tyro3 (Figure 7A). Axl and Mer expression was also evaluated to provide an indication of whether Gas6 may induce downstream Akt phosphorylation through an alternate receptor (Figure 7A).

Mouse Gas6-induced Tyro3 phosphorylation was observed in the hTyro3-transfected NIH-3T3 cell line and to a lesser extent in the SKMEL2 line (Figure 7B). The difference in the observed pTyro3 levels could be explained by the substantially lower level of expression of endogenous Tyro3 in SKMEL2 (Figure 1C) as opposed to the high Tyro3 levels within the recombinantly transfected NIH-3T3 cell line. Gas6-induced Akt phosphorylation could also be observed in the cell lines (Figure 7C; determination of the level of Gas6 required to induce Akt phosphorylation is described below). Akt phosphorylation was necessarily due to the presence of hTyro3 in the hTyro3-tranfected NIH-3T3 line because the untransfected cell line did not demonstrate visible Gas6-induced Akt phosphorylation. We tested the ability of Gas6 to induce phosphorylation of Akt and Erk (MAPK) in a wider panel of melanoma cells lines, as well as in a (colorectal cancer) cell line that lacked Tyro3 but expresses Axl (Figure 8A). In all the Tyro3-expressing cell lines, Gas6 significantly induced activation of Akt, and this effect was not affected by the mutation status of RAF and/or RAS. No ligand-induced Erk phosphorylation was observed in any of the lines (Figure 8A).

Biochemical Characterization of Mouse Anti-Tyro3 mAbs. Twenty hybridoma clones derived from fusion of B-cells from mice immunized with the hTyro3-ECD protein with Sp2/0 myeloma cells were used to produce mAbs. All the mAbs bound the human Tyro3 with low nanomolar to high picomolar EC_{50} values in a direct binding ELISA, and a few also bound the mouse receptor (Table 2). Each mAb was assessed for its ability to cross-block every other mAb in the panel using SPR (Figure S2A of the Supporting Information and Table 2). Eight clearly distinguishable epitope groups were defined by the cross-blocking data. Sibling analyses using a proteomic approach indicated that only four mAb pairs had similar germline variable domains [BI_1A11 and BI_5H4, BI_6F2 and BI_12D7, BI_16E12 and BI_17B11, and BI_5A4 and BI_10A1 (S. J. Demarest et al., unpublished data)]. Only two mAbs, BI_1A11 and BI_5H4 (siblings), demonstrated weak cross-reactivity with respect to Axl or Mer with apparent EC_{50} values >3 orders of magnitude weaker than those of the positive control mAbs directed against Axl or Mer (Table 2). Only five mAbs had epitopes that engaged the Tyro3 FnIII domains based on ELISA binding studies with the hTyro3-Ig protein (Table 2). Lastly, the ability of each mAb to block hTyro3 from binding hGas6 was assessed (Table 2). Examples of ELISA results demonstrating weak, partial, and strong ligand blocking mAbs are provided in Figure S2B of the Supporting Information. Only siblings BI_1A11 and BI_5H4 mAbs appeared to be purely competitive blockers (i.e., could bring the hGas6/hTyro3 ELISA signal to baseline). Many of the other mAbs demonstrated partial or weak ligand blocking capability, a phenomenon that can be associated with (i) epitopes near the ligand binding pocket or (ii) allosteric inhibition. Overall, the biochemical data indicate the panel of mAbs is diverse, recognizing eight clearly different epitopes, including epitopes on both the Ig domains and the FnIII domains. Diverse ligand blocking behaviors for mAbs that fully cross-block one another give indications of additional epitope diversity within the individual epitope groups defined by the cross-blocking experiments.

Antibody-Mediated Inhibition of Ligand-Induced Tyro3 Signaling. The anti-Tyro3 mAbs were tested for their ability to inhibit ligand-induced Akt phosphorylation. Both hGas6 and mGas6 were titrated onto MDA-MB-435S cells to generate a dose-dependent Akt phosphorylation curve. The apparent EC_{50} of hGas6 was ∼25−50 μg/mL [near the apparent affinity of 200 nM determined for the hGas6/hTyro3-ECD interaction described above (data not shown)]. The mGas6 protein was much more potent with an EC_{50} of ∼1 μg/mL based on Western blotting (Figure 8B), also in agreement with the higher potency observed for mGas6 in the biochemical biotin-Gas6/hTyro3 blocking ELISA. Similar results were obtained after stimulation for 10, 30, or 120 min. On the basis of these results, mGas6 was used to stimulate Akt phosphorylation after preincubation with the anti-Tyro3 mAbs.

Of the eight mAb epitope groups, two highly overlapping epitope groups were found to inhibit Tyro3-mediated Akt signaling. The mAbs were preincubated with MDA-MB-435, A2058, or SKMEL30 cells prior to Tyro3 (or Axl) stimulation by mGas6. The mAbs in the same category as 14B7 and 16E12 completely inhibited mGas6-induced Akt phosphorylation through Tyro3 in both MDA-MB-435 and SKMEL30 cells, both cell lines that lack Axl (Figure 7D). The mGas6-induced phosphorylation in A2058 was only partially inhibited likely because of mGas6 activation through Axl, which is not recognized by the mAbs (Figure 7D). The 14B7 and 16E12 mAbs also demonstrated the ability to reduce the level of Akt phosphorylation induced by FBS in MDA-MB-435S cells (Figure 7D), suggesting the possible inhibition of bovine PS-induced Tyro3 phosphorylation. For reference, results with untreated cells and cells treated with a neutral (nonactive) mAb, 7A2, are also shown (Figure 7D).

dx.doi.org/10.1021/bi301588c | *Biochemistry* 2013, 52, 3102−3118

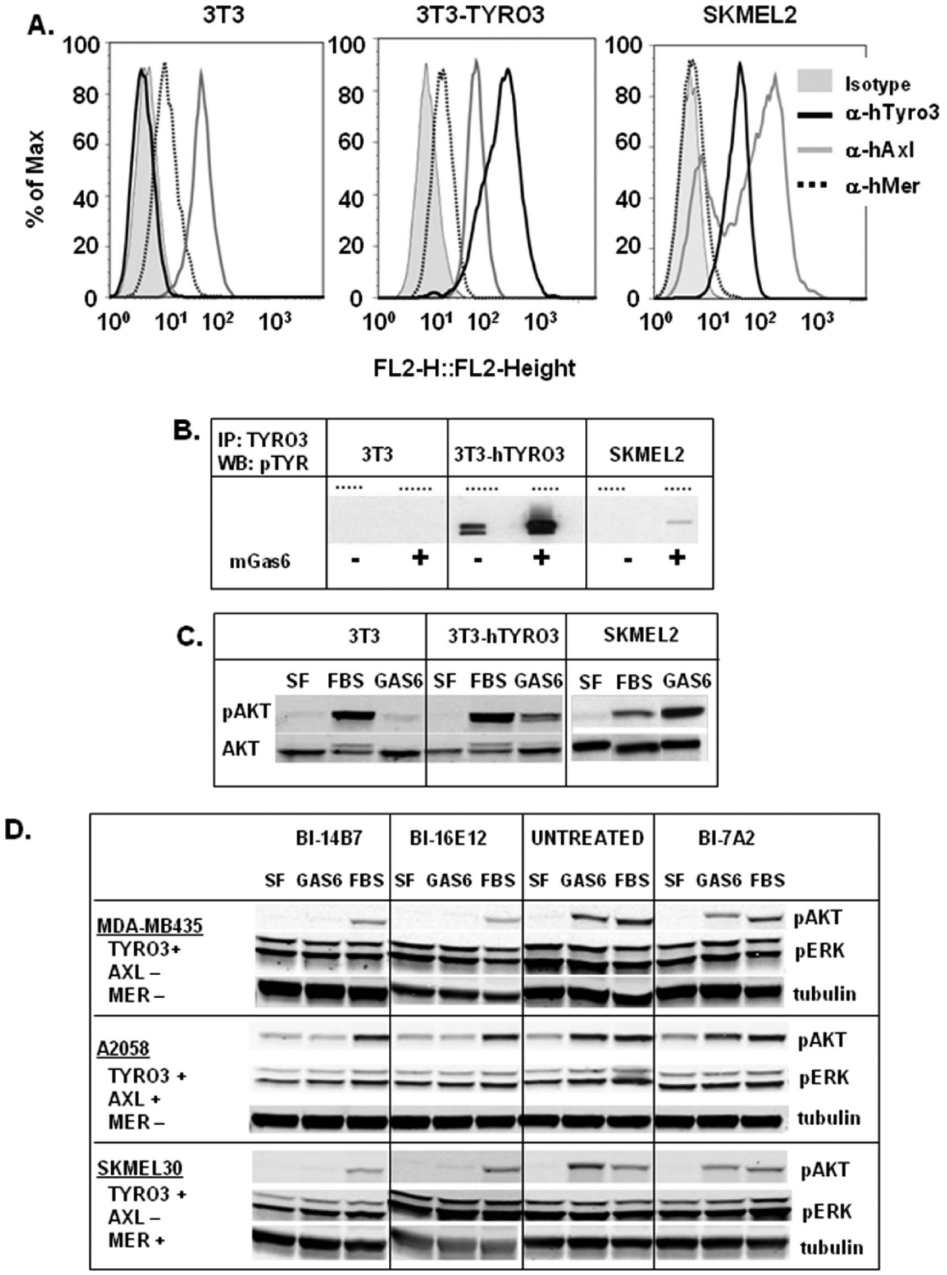

Figure 7. Ligand-mediated activation of Tyro3/Akt and mAb-dependent inhibition. (A) Tyro3, Axl, and Mer detection in NIH-3T3 cells untransfected or transfected with hTYRO3 (full-length receptor) and SKMEL2 by flow cytometry. (B) Immunoprecipitation of Tyro3 after no stimulation or stimulation with 400 ng/mL mGas6 in untransfected and hTYRO3-transfected NIH-3T3 cell lines and in SKMEL2. (C) Akt phosphorylation induced by FBS or mGas6 in the NIH-3T3-untransfected and hTyro3-transfected cell lines and in SKMEL2. (D) Preincubation of MDA-MB-435, A2058, and SKMEL30 melanoma cells with three representative anti-Tyro3 mAbs prior to the addition of FBS or 400 ng/mL mGas6. BI-14B7 and BI-16E12 are representatives of inhibitory mAbs, while BI-7A2 represents a neutral mAb.

DISCUSSION

Biochemistry of the Gas6–Tyro3 Interaction. Many of the data surrounding TAMRs have revolved around the Axl and Mer receptors, and their roles in biology are currently more defined than that of Tyro3. Both Gas6 and PS have been implicated as ligands for Tyro3, and there is some uncertainty regarding the relative strength of binding of Gas6 to Axl and Tyro3.[3] Here, we provide both quantitative and relative TAMR binding experiments that clearly demonstrate Gas6 and PS (albeit with a >10-fold weaker affinity) have the capacity to bind Tyro3 (Figures 5 and 6C). Our solution inhibition data (Figure 6D) provide affinities of the TAMRs for hGas6 (with Axl-Fc > Tyro3-Fc > Mer-Fc) and agree with previously reported results using ideal monomeric reagents to measure the interaction between Axl and Gas6 [K_D of 2.5 ± 1.5 nM (reported here) vs 4 nM (reported previously)].[39] The levels of hGas6 needed to activate hTyro3-mediated downstream phosphorylation of Akt correlated well with the apparent affinity of hGas6 for hTyro3. PS has been shown to be critical for various activities of Tyro3, including its role in neuronal protection.[6,9] On the basis of both Gas6 and PS's relatively low affinity (Figures 5 and 6C) compared with their concentrations found in serum (K_D values of 0.2 and >2 μM, respectively), it is likely that avidity components contribute to their activation of

dx.doi.org/10.1021/bi301588c | *Biochemistry* 2013, 52, 3102–3118

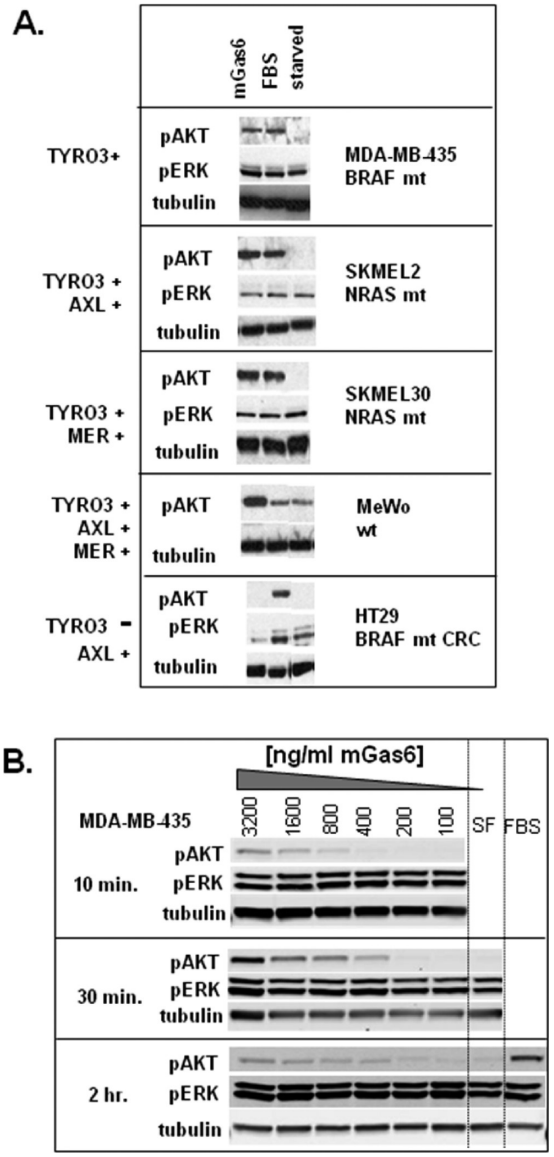

Figure 8. Gas6-induced Akt signaling in various tumor cell lines. (A) Akt phosphorylation induced by FBS or Gas6 in a variety of melanoma cell lines that differ in their TAMR expression patterns, as indicated. The lack of AKT phosphorylation observed in a Tyro3 negative cell line, the colorectal cancer cell line HT29, suggests that Gas6 specifically induces Akt phosphorylation through Tyro3, but not Axl. The RAS/RAF mutational status is indicated. (B) Titration of mGas6 into MDA-MB-435S cells with incubation for 10, 30, and 120 min. Titration with hGas6 was also performed, and the lower affinity of the ligand resulted in an IC_{50} of ~20 μg/mL (data not shown).

Tyro3. Perhaps the binding of the Gla region to cell surfaces may improve their effective concentration and ability to engage Tyro3.[3] Gas6 can be co-expressed within tumor cell lines that express Axl, and there is likely a similar mechanism for autocrine or paracrine expression-mediated ligand activation of Tyro3.[40,41] Strangely, the mouse protein binds human Tyro3 much more tightly than the human protein (Figure 5C), and mGas6 is incidentally often used to study the signaling of both Axl and Tyro3.

Calcium obviously facilitated binding of Gas6 to TAM receptors. Our data indicate Ca^{2+} significantly stabilizes Gas6 (Figure 4). The GLA region and LG domains of Gas6 have demonstrated Ca^{2+} binding.[3] Ca^{2+} coordination within the GLA region is an important mechanism for engaging negatively charged phospholipids found on the surfaces of apoptotic cells.[3] With regard to TAMR interactions, Ca^{2+} binding is thought to organize and/or restrict the interdomain motions of the C-terminal LG domains known to engage TAMRs.[38,39] Our data indicate Ca^{2+} binding is also important for Gas6 folding and likely reduces the necessity for induced folding during the binding of TAMRs.

Tyro3 Expression and Activity in Melanoma. The potential role of Tyro3 in melanoma has been a growing area of interest.[42] However, very little has been published regarding its role in melanoma since the initial publication of its high level of expression within melanoma cells and its potential connection with MITF.[29] Tyro3 has stood out in a number of recent studies that analyzed RTK expression in both melanoma and primary tumor samples.[30,43] We demonstrate frequent over-expression of Tyro3 in melanoma cell lines from the commercial ASCENTA (Figure 1A) and OriGene (Figure S1C of the Supporting Information) databases and within the publicly available mRNA gene expression database at the National Cancer Institute.[44] Additionally, Tyro3 protein was found in all the tumor cell lines we assessed by FACS and Western blotting (Figure 1B). Axl, on the other hand, appears not to be commonly expressed in melanoma (normal melanocytes were not available for analysis). Unlike those of oncogenic RTKs like HER-2/neu or c-Met,[45,46] Tyro3 levels were not extremely high in melanoma. While the OriGene database indicated that the level of Tyro3 expression was roughly 350% above normal (only three normal samples), the level of Tyro3 was only 50% above the normal tissue baseline in the ASCENTA database and 100% above its average level across other tumor types with no radically upregulated exceptions.[44] The trend, however, of higher levels of expression in melanoma is strong. The knockdown data (Figure 1B) clearly suggest the importance of Tyro3 in melanoma because all 12 of the melanoma cell lines transduced with the Tyro3-specific shRNA displayed some cell death, with 8 of 12 demonstrating high levels (>75%) of cell death. There was no correlation between Tyro3 expression level and the sensitivity to shRNA knockdown, possibly because of co-expression of other growth factor receptors, differential activation of other survival genes, and/or other (epi)genetic mechanisms specific to each melanoma cell line, which warrants additional future investigations into this phenomenon. We also show that ligand-mediated Tyro3 signaling in Tyro3-positive (Axl-negative) melanoma lines leads to both Tyro3 (Figure 7B) and downstream Akt (Figure 8B) phosphorylation, perhaps contributing to the cells' ability to survive. Zhu and co-workers demonstrated that Tyro3 knockdown led to MITF down-regulation and cell death in multiple melanoma cell lines, as well as a reduced level of tumor formation *in vivo*.[29] MITF has been identified as a lineage survival oncogene in melanoma that protects cells from undergoing apoptosis in the presence of chemotherapeutics.[44] Tyro3's link to MITF may be a second survival mechanism. Inhibiting the survival pathway through Tyro3 blockade may provide a useful component within combination strategies for overcoming resistance mechanisms arising in melanoma patients with B-Raf mutations after treatment with B-Raf inhibitors.

Tyro3-Specific mAbs as Tools for Evaluating the Importance of Tyro3 in Melanoma. Generally, mAb-specific inhibition of RTK activity can be accomplished through allosteric or competitive ligand blockade, through degradation

dx.doi.org/10.1021/bi301588c | *Biochemistry* 2013, 52, 3102−3118

Table 2. Characterization of Ig Domain or FnIII Domain Binding, Species Cross-Reactivity (mouse and human), Ligand Blocking Capacity, and mAb Cross-Reactivity of the Anti-Tyro3 mAbs[a]

clone	mAb	Axl/Mer cross-reactivity	hTyro3-ECD [EC_{50} (nM)]	hTyro3-Ig [EC_{50} (nM)]	mTyro3-ECD-Fc [EC_{50} (nM)]	hGas6 blocking[b]	cross-block clones
BI_1A11	1	weak	0.2	0.24	N[c]	**strong**	**1, 7**
BI_5H4	7	weak	0.27	0.26	N[c]	**strong**	**1, 7**
BI_20A4	19	N[c]	0.18	0.12	N[c]	weak	3, 19
BI_1E8	3	N[c]	0.88	1	N[c]	none	**2,[d] 3, 5,[d] 13,[d] 14,[d] 16,[d] 19**
BI_7A2	9	N[c]	0.21	**no**	N[c]	none	9, 20
BI_20B7	20	N[c]	0.2	**58**	N[c]	weak	9, 20
BI_4D4	5	N[c]	0.15	0.27	N[c]	none	**2, 3,[d] 4, 5, 8, 11−14, 16−18**
BI_14B7	12	N[c]	0.08	0.1	N[c]	partial	**2, 3,[d] 4, 5, 8, 11−14, 16−18**
BI_14E1	13	N[c]	0.16	0.18	N[c]	partial	**2, 3,[d] 4, 5, 8, 11−14, 16−18**
BI_16D11	16	N[c]	0.08	0.05	N[c]	partial	**2, 3,[d] 4, 5, 8, 11−14, 16−18**
BI_1E1	2	N[c]	0.17	0.23	N[c]	partial	2, 4, 5, 8, 11−14, 16−18
BI_3E6	4	N[c]	0.07	0.12	N[c]	weak	2, 4, 5, 8, 11−14, 16−18
BI_6F2	8	N[c]	0.16	0.32	N[c]	weak	2, 4, 5, 8, 11−14, 16−18
BI_12D7	11	N[c]	0.11	0.09	N[c]	partial	2, 4, 5, 8, 11−14, 16−18
BI_14F5	14	N[c]	0.13	0.11	N[c]	none	2, 4, 5, 8, 11−14, 16−18
BI_16E12	17	N[c]	0.09	0.04	N[c]	weak	2, 4, 5, 8, 11−14, 16−18
BI_17B11	18	N[c]	0.1	0.03	N[c]	weak	2, 4, 5, 8, 11−14, 16−18
BI_16A5	15	N[c]	0.18	**320**	**0.12**	partial	**15**
BI_5A4	6	N[c]	0.26	**no**	**0.09**	weak	6, 10
BI_10A1	10	N[c]	0.12	**no**	**0.09**	weak	6, 10
R&D 859			0.13	0.18	N[c]	partial	

[a]Bold font highlights unique aspects of various epitope classes and more clearly highlights the different epitope classes in the cross-blocking column. [b]Percent of ligand blocked at saturating levels of mAb based on ELISA: none, <20%; weak, between 21 and 50%; partial, between 51 and 80%; strong, >80%. [c]Did not bind. [d]The level of clone binding was reduced but not eliminated.

or internalization of the receptors, through inhibition of the formation of signaling complexes, or by the external arrangement of the tyrosine kinase domains to adopt a nonsignaling conformation. Some of these activities are more easily observed than others, and the best inhibitory mechanisms clearly differ across varying receptor types. The Tyro3-specific mAbs described here have a wide array of ligand blocking capabilities. For Tyro3, the ability to block ligand did not correlate well with the ability to most effectively block downstream signaling (Table 2 and Figure 7C), but some trends were clear. Two epitope families directed at the FnIII domains of the extracellular domains had no impact on receptor signaling. Surprisingly, the competitive blockers, which bound the Ig domains of Tyro3, displayed only a weak ability to block ligand-mediated Akt signaling, perhaps acting as weak agonists themselves after blocking Gas6 from binding Tyro3. It was mAbs targeting the Ig domains, but with partial ligand blocking ability, that were capable of completely blocking ligand-mediated downstream receptor signaling. Axl mAbs targeting the Ig domains of Axl have also been shown to block the activity of this receptor.[20] The molecular mechanism(s) for how these mAbs inhibit receptor signaling will await further studies, and the panel of mAbs described here will serve as a useful tool for studying the possible activity of Tyro3 in melanoma and other diseases.

■ ASSOCIATED CONTENT

Supporting Information

mRNA expression analyses of TYRO3, AXL, and MER in both normal and disease tissues and representative data from the biochemical characterization of the anti-Tyro3 mAbs. This material is available free of charge via the Internet at http://pubs.acs.org.

■ AUTHOR INFORMATION

Corresponding Author

*S.J.D.: current address, Lilly Biotechnology Center, 10300 Campus Point Dr., San Diego, CA 92121; telephone, (858) 638-8634; e-mail, demarestsj@lilly.com. L.A.K.: current address, Celgene Avilomics Research, 45 Wiggins Ave., Bedford, MA 01730; telephone, (617) 230-4822; e-mail, lkoopman@celgene.com.

Present Addresses

[†]M.C.V.: Pfizer, 10770 Science Center Dr., San Diego, CA 92121.

[‡]E.A.: Sorrento Therapeutics, 6042 Cornerstone Ct. W., Suite B, San Diego, CA 92121.

Notes

The authors declare no competing financial interest.

■ ACKNOWLEDGMENTS

We thank Dr. Kristin Demarest for critical reading of the manuscript.

■ ABBREVIATIONS

CHO, Chinese hamster ovary; DSC, differential scanning calorimetry; FACS, fluorescence-activated cell sorting; FBS, fetal bovine serum; mAb, monoclonal antibody; PBS, phosphate-buffered saline; PS, protein S; RTK, receptor

tyrosine kinase; RU, resonance unit; SEC, size exclusion chromatography; shRNA, short hairpin ribonucleic acid; SPR, surface plasmon resonance.

REFERENCES

(1) Lemke, G., and Rothlin, C. V. (2008) Immunobiology of the TAM receptors. *Nat. Rev. Immunol. 8*, 327−336.

(2) Stitt, T. N., Conn, G., Gore, M., Lai, C., Bruno, J., Radziejewski, C., Mattsson, K., Fisher, J., Gies, D. R., Jones, P. F., et al. (1995) The anticoagulation factor protein S and its relative, Gas6, are ligands for the Tyro 3/Axl family of receptor tyrosine kinases. *Cell 80*, 661−670.

(3) Hafizi, S., and Dahlback, B. (2006) Gas6 and protein S: Vitamin K-dependent ligands for the Axl receptor tyrosine kinase subfamily. *FEBS J. 273*, 5231−5244.

(4) Linger, R. M., Keating, A. K., Earp, H. S., and Graham, D. K. (2008) TAM receptor tyrosine kinases: Biologic functions, signaling, and potential therapeutic targeting in human cancer. *Adv. Cancer Res. 100*, 35−83.

(5) Lan, Z., Wu, H., Li, W., Wu, S., Lu, L., Xu, M., and Dai, W. (2000) Transforming activity of receptor tyrosine kinase Tyro3 is mediated, at least in part, by the PI3 kinase-signaling pathway. *Blood 95*, 633−638.

(6) Zhong, Z., Wang, Y., Guo, H., Sagare, A., Fernandez, J. A., Bell, R. D., Barrett, T. M., Griffin, J. H., Freeman, R. S., and Zlokovic, B. V. (2010) Protein S protects neurons from excitotoxic injury by activating the TAM receptor Tyro3-phosphatidylinositol 3-kinase-Akt pathway through its sex hormone-binding globulin-like region. *J. Neurosci. 30*, 15521−15534.

(7) Lu, Q., Gore, M., Zhang, Q., Camenisch, T., Boast, S., Casagranda, F., Lai, C., Skinner, M. K., Klein, R., Matsushima, G. K., Earp, H. S., Goff, S. P., and Lemke, G. (1999) Tyro-3 family receptors are essential regulators of mammalian spermatogenesis. *Nature 398*, 723−728.

(8) Lu, Q., and Lemke, G. (2001) Homeostatic regulation of the immune system by receptor tyrosine kinases of the Tyro 3 family. *Science 293*, 306−311.

(9) Lemke, G., and Burstyn-Cohen, T. (2010) TAM receptors and the clearance of apoptotic cells. *Ann. N.Y. Acad. Sci. 1209*, 23−29.

(10) Gal, A., Li, Y., Thompson, D. A., Weir, J., Orth, U., Jacobson, S. G., Apfelstedt-Sylla, E., and Vollrath, D. (2000) Mutations in MERTK, the human orthologue of the RCS rat retinal dystrophy gene, cause retinitis pigmentosa. *Nat. Genet. 26*, 270−271.

(11) Rothlin, C. V., Ghosh, S., Zuniga, E. I., Oldstone, M. B., and Lemke, G. (2007) TAM receptors are pleiotropic inhibitors of the innate immune response. *Cell 131*, 1124−1136.

(12) Zhu, D., Wang, Y., Singh, I., Bell, R. D., Deane, R., Zhong, Z., Sagare, A., Winkler, E. A., and Zlokovic, B. V. (2010) Protein S controls hypoxic/ischemic blood-brain barrier disruption through the TAM receptor Tyro3 and sphingosine 1-phosphate receptor. *Blood 115*, 4963−4972.

(13) Prieto, A. L., O'Dell, S., Varnum, B., and Lai, C. (2007) Localization and signaling of the receptor protein tyrosine kinase Tyro3 in cortical and hippocampal neurons. *Neuroscience 150*, 319−334.

(14) Nakamura, Y. S., Hakeda, Y., Takakura, N., Kameda, T., Hamaguchi, I., Miyamoto, T., Kakudo, S., Nakano, T., Kumegawa, M., and Suda, T. (1998) Tyro 3 receptor tyrosine kinase and its ligand, Gas6, stimulate the function of osteoclasts. *Stem Cells 16*, 229−238.

(15) Zhang, Z., Lee, J. C., Lin, L., Olivas, V., Au, V., LaFramboise, T., Abdel-Rahman, M., Wang, X., Levine, A. D., Rho, J. K., Choi, Y. J., Choi, C. M., Kim, S. W., Jang, S. J., Park, Y. S., Kim, W. S., Lee, D. H., Lee, J. S., Miller, V. A., Arcila, M., Ladanyi, M., Moonsamy, P., Sawyers, C., Boggon, T. J., Ma, P. C., Costa, C., Taron, M., Rosell, R., Halmos, B., and Bivona, T. G. (2012) Activation of the AXL kinase causes resistance to EGFR-targeted therapy in lung cancer. *Nat. Genet. 44*, 852−860.

(16) Mahadevan, D., Cooke, L., Riley, C., Swart, R., Simons, B., Della Croce, K., Wisner, L., Iorio, M., Shakalya, K., Garewal, H., Nagle, R., and Bearss, D. (2007) A novel tyrosine kinase switch is a mechanism of imatinib resistance in gastrointestinal stromal tumors. *Oncogene 26*, 3909−3919.

(17) Liu, L., Greger, J., Shi, H., Liu, Y., Greshock, J., Annan, R., Halsey, W., Sathe, G. M., Martin, A. M., and Gilmer, T. M. (2009) Novel mechanism of lapatinib resistance in HER2-positive breast tumor cells: Activation of AXL. *Cancer Res. 69*, 6871−6878.

(18) Hong, C. C., Lay, J. D., Huang, J. S., Cheng, A. L., Tang, J. L., Lin, M. T., Lai, G. M., and Chuang, S. E. (2008) Receptor tyrosine kinase AXL is induced by chemotherapy drugs and overexpression of AXL confers drug resistance in acute myeloid leukemia. *Cancer Lett. 268*, 314−324.

(19) Li, Y., Ye, X., Tan, C., Hongo, J. A., Zha, J., Liu, J., Kallop, D., Ludlam, M. J., and Pei, L. (2009) Axl as a potential therapeutic target in cancer: Role of Axl in tumor growth, metastasis and angiogenesis. *Oncogene 28*, 3442−3455.

(20) Ye, X., Li, Y., Stawicki, S., Couto, S., Eastham-Anderson, J., Kallop, D., Weimer, R., Wu, Y., and Pei, L. (2010) An anti-Axl monoclonal antibody attenuates xenograft tumor growth and enhances the effect of multiple anticancer therapies. *Oncogene 29*, 5254−5264.

(21) Holland, S. J., Pan, A., Franci, C., Hu, Y., Chang, B., Li, W., Duan, M., Torneros, A., Yu, J., Heckrodt, T. J., Zhang, J., Ding, P., Apatira, A., Chua, J., Brandt, R., Pine, P., Goff, D., Singh, R., Payan, D. G., and Hitoshi, Y. (2010) R428, a selective small molecule inhibitor of Axl kinase, blocks tumor spread and prolongs survival in models of metastatic breast cancer. *Cancer Res. 70*, 1544−1554.

(22) Eder, J. P., Shapiro, G. I., Appleman, L. J., Zhu, A. X., Miles, D., Keer, H., Cancilla, B., Chu, F., Hitchcock-Bryan, S., Sherman, L., McCallum, S., Heath, E. I., Boerner, S. A., and LoRusso, P. M. (2010) A phase I study of foretinib, a multi-targeted inhibitor of c-Met and vascular endothelial growth factor receptor 2. *Clin. Cancer Res. 16*, 3507−3516.

(23) Yakes, F. M., Chen, J., Tan, J., Yamaguchi, K., Shi, Y., Yu, P., Qian, F., Chu, F., Bentzien, F., Cancilla, B., Orf, J., You, A., Laird, A. D., Engst, S., Lee, L., Lesch, J., Chou, Y. C., and Joly, A. H. (2011) Cabozantinib (XL184), a Novel MET and VEGFR2 Inhibitor, Simultaneously Suppresses Metastasis, Angiogenesis, and Tumor Growth. *Mol. Cancer Ther. 10*, 2298−2308.

(24) Lai, C., Gore, M., and Lemke, G. (1994) Structure, expression, and activity of Tyro 3, a neural adhesion-related receptor tyrosine kinase. *Oncogene 9*, 2567−2578.

(25) Crosier, P. S., Hall, L. R., Vitas, M. R., Lewis, P. M., and Crosier, K. E. (1995) Identification of a novel receptor tyrosine kinase expressed in acute myeloid leukemic blasts. *Leuk. Lymphoma 18*, 443−449.

(26) Grueneberg, D. A., Degot, S., Pearlberg, J., Li, W., Davies, J. E., Baldwin, A., Endege, W., Doench, J., Sawyer, J., Hu, Y., Boyce, F., Xian, J., Munger, K., and Harlow, E. (2008) Kinase requirements in human cells: I. Comparing kinase requirements across various cell types. *Proc. Natl. Acad. Sci. U.S.A. 105*, 16472−16477.

(27) Lan, Z., Wu, H., Li, W., Wu, S., Lu, L., Xu, M., and Dai, W. (2000) Transforming activity of receptor tyrosine kinase tyro3 is mediated, at least in part, by the PI3 kinase-signaling pathway. *Blood 95*, 633−638.

(28) Rikova, K., Guo, A., Zeng, Q., Possemato, A., Yu, J., Haack, H., Nardone, J., Lee, K., Reeves, C., Li, Y., Hu, Y., Tan, Z., Stokes, M., Sullivan, L., Mitchell, J., Wetzel, R., Macneill, J., Ren, J. M., Yuan, J., Bakalarski, C. E., Villen, J., Kornhauser, J. M., Smith, B., Li, D., Zhou, X., Gygi, S. P., Gu, T. L., Polakiewicz, R. D., Rush, J., and Comb, M. J. (2007) Global survey of phosphotyrosine signaling identifies oncogenic kinases in lung cancer. *Cell 131*, 1190−1203.

(29) Zhu, S., Wurdak, H., Wang, Y., Galkin, A., Tao, H., Li, J., Lyssiotis, C. A., Yan, F., Tu, B. P., Miraglia, L., Walker, J., Sun, F., Orth, A., Schultz, P. G., and Wu, X. (2009) A genomic screen identifies TYRO3 as a MITF regulator in melanoma. *Proc. Natl. Acad. Sci. U.S.A. 106*, 17025−17030.

(30) Tworkoski, K., Singhal, G., Szpakowski, S., Zito, C. I., Bacchiocchi, A., Muthusamy, V., Bosenberg, M., Krauthammer, M., Halaban, R., and Stern, D. F. (2011) Phosphoproteomic screen

identifies potential therapeutic targets in melanoma. *Mol. Cancer Res. 9*, 801−812.
(31) Avilla, E., Guarino, V., Visciano, C., Liotti, F., Svelto, M., Krishnamoorthy, G., Franco, R., and Melillo, R. M. (2011) Activation of TYRO3/AXL tyrosine kinase receptors in thyroid cancer. *Cancer Res. 71*, 1792−1804.
(32) Nagata, K., Ohashi, K., Nakano, T., Arita, H., Zong, C., Hanafusa, H., and Mizuno, K. (1996) Identification of the product of growth arrest-specific gene 6 as a common ligand for Axl, Sky, and Mer receptor tyrosine kinases. *J. Biol. Chem. 271*, 30022−30027.
(33) Brezinsky, S. C., Chiang, G. G., Szilvasi, A., Mohan, S., Shapiro, R. I., MacLean, A., Sisk, W., and Thill, G. (2003) A simple method for enriching populations of transfected CHO cells for cells of higher specific productivity. *J. Immunol. Methods 277*, 141−155.
(34) He, X., Shen, L., and Dahlback, B. (1995) Expression and functional characterization of chimeras between human and bovine vitamin-K-dependent protein-S-defining modules important for the species specificity of the activated protein C cofactor activity. *Eur. J. Biochem. 227*, 433−440.
(35) Grueneberg, D. A., Li, W., Davies, J. E., Sawyer, J., Pearlberg, J., and Harlow, E. (2008) Kinase requirements in human cells: IV. Differential kinase requirements in cervical and renal human tumor cell lines. *Proc. Natl. Acad. Sci. U.S.A. 105*, 16490−16495.
(36) Pearlberg, J., Degot, S., Endege, W., Park, J., Davies, J., Gelfand, E., Sawyer, J., Conery, A., Doench, J., Li, W., Gonzalez, L., Boyce, F. M., Brizuela, L., Labaer, J., Grueneberg, D., and Harlow, E. (2005) Screens using RNAi and cDNA expression as surrogates for genetics in mammalian tissue culture cells. *Cold Spring Harbor Symp. Quant. Biol. 70*, 449−459.
(37) Moffat, J., Grueneberg, D. A., Yang, X., Kim, S. Y., Kloepfer, A. M., Hinkle, G., Piqani, B., Eisenhaure, T. M., Luo, B., Grenier, J. K., Carpenter, A. E., Foo, S. Y., Stewart, S. A., Stockwell, B. R., Hacohen, N., Hahn, W. C., Lander, E. S., Sabatini, D. M., and Root, D. E. (2006) A lentiviral RNAi library for human and mouse genes applied to an arrayed viral high-content screen. *Cell 124*, 1283−1298.
(38) Sasaki, T., Knyazev, P. G., Cheburkin, Y., Gohring, W., Tisi, T., et al. (2002) Crystal structure of a C-terminal fragment of growth arrest-specific protein Gas6. *J. Biol. Chem. 277*, 44164−44170.
(39) Sasaki, T., Knyazev, P. G., Clout, N. J., Cheburkin, Y., Gohring, W., Ullrich, A., Timpl, R., and Hohenester, E. (2006) Structural basis for Gas6-Axl signalling. *EMBO J. 25*, 80−87.
(40) Shiozawa, Y., Pedersen, E. A., Patel, L. R., Ziegler, A. M., Havens, A. M., Jung, Y., Wang, J., Zalucha, S., Loberg, R. D., Pienta, K. J., and Taichman, R. S. (2010) GAS6/AXL axis regulates prostate cancer invasion, proliferation, and survival in the bone marrow niche. *Neoplasia 12*, 116−127.
(41) Sensi, M., Catani, M., Castellano, G., Nicolini, G., Alciato, F., Tragni, G., De Santis, G., Bersani, I., Avanzi, G., Tomassetti, A., Canevari, S., and Anichini, A. (2011) Human cutaneous melanomas lacking MITF and melanocyte differentiation antigens express a functional Axl receptor kinase. *J. Invest. Dermatol. 131*, 2448−2457.
(42) Rudloff, U., and Samuels, Y. (2010) TYRO3-mediated regulation of MITF: A novel target in melanoma? *Pigm. Cell Melanoma Res 23*, 9−11.
(43) Molheok, K., Shada, A., Smolkin, M., Chowbina, S., Papin, J., Brautigan, D., and Slingluff, C. J. (2011) Comprehensive analysis of receptor tyrosine kinase activation in human melanomas reveals autocrine signaling through IGF-1R. *Melanoma Res. 21*, 274−284.
(44) Garraway, L. A., Widlund, H. R., Rubin, M. A., Getz, G., Berger, A. J., Ramaswamy, S., Beroukhim, R., Milner, D. A., Granter, S. R., Du, J., Lee, C., Wagner, S. N., Li, C., Golub, T. R., Rimm, D. L., Meyerson, M. L., Fisher, D. E., and Sellers, W. R. (2005) Integrative genomic analyses identify MITF as a lineage survival oncogene amplified in malignant melanoma. *Nature 436*, 117−122.
(45) Press, M. F., Jones, L. A., Godolphin, W., Edwards, C. L., and Slamon, D. J. (1990) HER-2/neu oncogene amplification and expression in breast and ovarian cancers. *Prog. Clin. Biol. Res. 354A*, 209−221.
(46) Comoglio, P. M., Giordano, S., and Trusolino, L. (2008) Drug development of MET inhibitors: Targeting oncogene addiction and expedience. *Nat. Rev. Drug Discovery 7*, 504−516.